PORTLAND PRESS

Research Article

Cyanobacterial redox carriers support photosynthesis in a purple phototrophic bacterium

Adam G.M. Bowie[1] [iD], Andrew Hitchcock[1,2] [iD], Matthew S. Proctor[1] [iD], Elizabeth C. Martin[1] [iD], David J.K. Swainsbury[3] [iD] and C. Neil Hunter[1] [iD]

[1]Plants, Photosynthesis and Soil, School of Biosciences, University of Sheffield, Sheffield, UK; [2]Molecular Microbiology: Biochemistry to Disease, School of Biosciences, University of Sheffield, Sheffield, UK; [3]School of Biological Sciences, University of East Anglia, Norwich Research Park, Norwich, UK

Correspondence: Andrew Hitchcock (a.hitchcock@sheffield.ac.uk) and C. Neil Hunter (c.n.hunter@sheffield.ac.uk)

OPEN ACCESS

In oxygenic and anoxygenic photosynthesis, excitation energy migrates from a surrounding antenna to specialised chlorophyll (Chl) or bacteriochlorophyll (BChl) pigments housed within a reaction centre (RC) complex. Here, a charge-separated state is formed within a few picoseconds, and an electron moves along a series of cofactors until it arrives at a quinone or iron–sulphur centre acceptor. Further photochemical cycles rely on rapid re-reduction in the photo-oxidised RC, usually by small, soluble metalloproteins which vary considerably between different phototrophic clades. In the purple phototrophic bacterium *Rhodobacter* (*Rba*.) *sphaeroides*, the electron carrier cytochrome c_2 (cyt c_2) shuttles between the periplasmic faces of the cytochrome bc_1 complex and the reaction centre-light harvesting 1 (RC-LH1) core complex, the location of the BChl special pair (P_{865}). By contrast, in the model cyanobacterium *Synechocystis* sp. PCC 6803, electrons are transferred from cytochrome b_6f to photosystem I (PSI) via two isofunctional redox carrier proteins, cytochrome c_6 (cyt c_6) or plastocyanin (Pc). In the present study, we demonstrate that both cyt c_6 and Pc can substitute for cyt c_2 *in silico*, *in vitro* and *in vivo*, even though their electrostatic properties may be counter-productive for binding the RC-LH1 complex. Interestingly, whilst P_{865}^+ reduction was highest with cyt c_2 and the full physiological RC-LH1 complex, both *Synechocystis* proteins were more compatible with the RC-only complex lacking the surrounding LH1 antenna. Taken together, this suggests the subunits that constitute the LH1 ring improve both the donor side activity and selectivity of the *Rba. sphaeroides* RC complex.

Introduction

Oxygenic and anoxygenic photosynthesis are powered by spectrally distinct reaction centres (RCs) that share a common evolutionary origin [1–4]. This relatedness is evident from the structural homology between the five core transmembrane helices of all extant RCs, but after billions of years of divergent evolution, modern RC complexes share little meaningful sequence identity [2]. Some RCs use bacteriochlorophylls (BChls) as their primary charge-separating pigments, whilst others harness chlorophylls (Chls), but their electron acceptors are the basis for delineating two RC classes. Following photochemical charge separation, Type I (Fe–S type) RCs pass electrons to iron–sulfur clusters via either of the two (pseudo)symmetric branches of cofactors, whereas type II (Q-type) RCs reduce quinone acceptors via the active branch (A-branch) of cofactors [1]. There are also differences in the way electrons are supplied to the photo-oxidised primary pigments, resetting RCs for further rounds of photochemistry. The electron donors to both type I and type II RCs in the photo-oxidised state are generally small, mobile electron carriers such as *c*-type cytochromes or plastocyanin (Pc), with the notable exception of photosystem II (PSII) in cyanobacteria, algae and plants, which has evolved the capacity to extract electrons from water, generating oxygen as a 'waste' by-product [5,6]. The green or purple phototrophic bacterial clades make either type I or type II RCs, respectively, and have relatively simple, cyclic photosynthetic electron transfer chains, whereas cyanobacteria, algae and plants evolved the ability to assemble both RC types, specifically photosystem I (PSI) and the water-oxidising PSII complex [7]. Consequently, oxygenic photosynthesis employs a linear electron transfer pathway that couples PSII, cytochrome b_6f (cyt b_6f) and PSI complexes so that electrons from water are eventually used to reduce CO_2 to simple carbohydrates [8].

Photosynthetic organisms occupy specific spectral niches related to the light-absorbing pigments they produce. Purple phototrophic bacteria synthesising BChl *a* harvest near-infrared light in the 750–950 nm spectral region, whereas oxygenic phototrophs equipped with PSI and PSII use Chls to harvest visible light below 750 nm. This kind of specialisation has led to proposals to combine the attributes of both Chl- and BChl-containing RC complexes in a host organism, generating a hybrid, light-driven electron transfer system with an expanded spectral range able to absorb nearly all photosynthetically active solar radiation [9,10]. The native arrangement of the PSII and PSI complexes, both of which bind Chl *a*, was suggested to be inherently inefficient because both photosystems compete for the same photons [9]. Their vision of re-engineered photosynthesis replaced Chl *a*-containing PSI with a BChl *b*-based RC complex termed 'RC1', creating a more efficient photochemical system with complementary light absorption properties and minimal spectral overlap [9]. A subsequent proposal also replaced PSI with a BChl *b*-containing type II RC that drives an electron transfer loop involving the cyt *b_6f* complex, resembling cyclic electron transport in phototrophic bacteria. This new arrangement would generate a protonmotive force that drives the ATP synthase, whilst NADP$^+$ could be reduced by the NAD(P)H dehydrogenase complex operating in reverse [10].

A more recent proposal [11,12], depicted in Figure 1, retains the native PSII and PSI photosystems whilst introducing a new BChl *a*-based type II RC complex termed 'PSIII', forming a three-photosystem hybrid array that can utilise the visible, red, far-red and near-infrared regions of the solar spectrum. In this arrangement, intended to operate in a minimal cyanobacterial chassis [17], an engineered BChl-PSIII and the native Chl-PSI complex would compete for the same electron donors, cyt c_6 and Pc, with the relative electron flux through the two RCs being determined by whether the chromatic environment preferentially excites either Chl or BChl [11]. A minimally effective PSIII complex could be optimised by using adaptive laboratory evolution (ALE), which has already been used to introduce new traits in photosynthetic organisms such as high-light tolerance [18,19].

The list of modifications and genetic manipulations required to assemble a purple bacterial RC complex in a cyanobacterial chassis is formidable, particularly the heterologous expression of reaction centre-light harvesting 1 (RC-LH1) structural genes alongside their assembly factors and the wholesale rewiring of pigment biosynthesis pathways to make both Chl and BChl simultaneously [11]. Using the well-characterised RC complex from *Rba. sphaeroides* as a starting point for PSIII, extensive protein engineering would also be required to make the complex compatible with the native cyanobacterial photosynthetic machinery, reducing plastoquinone instead of ubiquinone (UQ) and oxidising cyt c_6 and Pc rather than cyt c_2. To investigate the feasibility of a PSIII complex, we have determined the level of
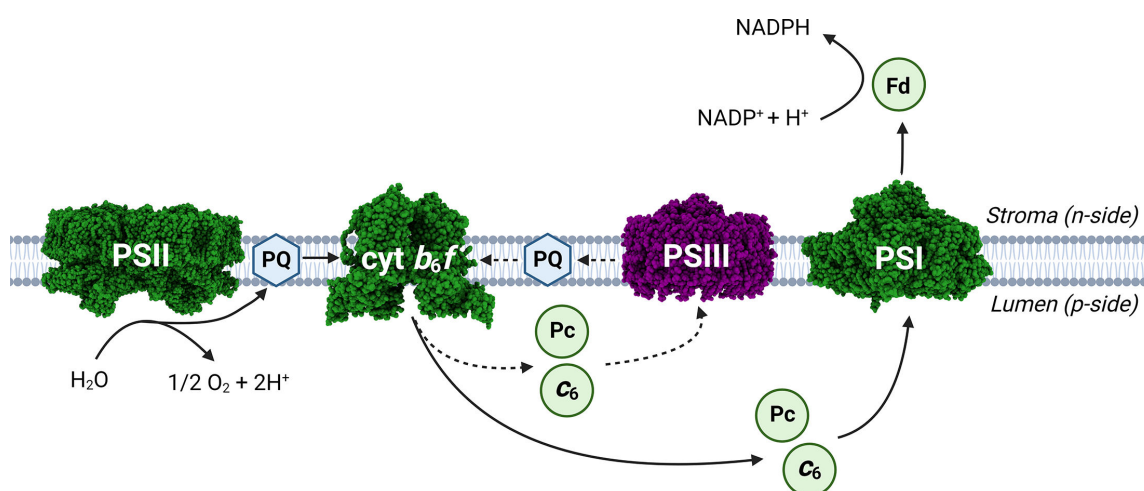
Figure 1: Envisaged three-photosystem electron transport chain in a transgenic cyanobacterium.

Electron transport pathways in a 'photo-redesigned' thylakoid membrane, as proposed by Hitchcock et al. [11], with native electron transfer proteins depicted in green and a near-infrared absorbing third photosystem ('PSIII') based on the reaction centre-light harvesting 1 (RC-LH1) complex of purple bacteria (coloured purple). This heavily redesigned complex would oxidise cytochrome c_6 (cyt c_6)/plastocyanin (Pc) and pass photoexcited electrons to plastoquinone (PQ), forming an additional cyclic electron transfer loop with cytochrome b_6f (cyt b_6f) (dashed lines) that contributes to thylakoid lumen acidification and ATP production. Space-filling models are included for photosystem I (PSI) [13], photosystem II (PSII) [14], cyt b_6f [15] and RC-LH1 [16] structures; host cyclic electron transfer is omitted for clarity.

pre-existing compatibility at the donor side of the *Rhodobacter* (*Rba.*) *sphaeroides* RC complex for binding the native cyt c_2 relative to cyt c_6 and Pc counterparts from *Synechocystis* sp. PCC 6803.

PSI and RC-LH1 accept electrons from soluble redox carrier proteins at binding sites that can be divided into two regions with different properties. In both RC types, a short-range interaction domain composed primarily of hydrophobic residues acts as the site of electron transfer, located on a pair of antiparallel helices that lie directly above the primary charge-separating pair of (B)Chls [3,20,21]. This region interacts with the face of the incoming electron donor through a series of van der Waals (vdW) contacts, hydrogen bonds and cation-π interactions, which are centred around a functionally imperative aromatic electron tunnelling contact, Tyr-L162 in RC-LH1 [20,22,23], and a pair of π-stacked tryptophan residues in PSI [24–26]. By contrast, a long-range interaction domain is formed by more distal charged residues making a series of complementary electrostatic interactions that steer the redox carrier protein towards its target via a transient encounter complex [20,27,28]. The balance between these two domains is different in the two RC complexes. The PSI interface is simpler and more symmetrical, being dominated by hydrophobic interactions and two arginine–aspartate charge pairs, whilst the RC-LH1 binding site has a much larger electrostatic component, featuring a ring of amino acids with negatively charged side chains [20,28,29].

The compartmentalisation of hydrophobic and charged residues is also apparent in the structures of the redox carrier proteins. In the class I *c*-type cytochromes cyt c_2 and cyt c_6, uncharged residues border the leading edge of the heme *c* prosthetic group, whilst in the blue copper protein Pc, a non-polar patch of residues known as the 'northern face' surrounds His-86, a key amino acid known to be part of the electron transfer pathway to PSI [30–32]. An outer ring of positively charged residues in cyt c_2 makes electrostatic interactions with RC-LH1, whilst cyt c_6 and Pc have acidic patches for interactions with PSI [25,32–34], although the eukaryotic homologues of these two proteins have much greater negative charge density due to electrostatic interactions with PsaF that are absent from cyanobacteria [25,30,35–37]. These differences in donor–acceptor binding interfaces between PSI, RC-LH1 and their respective electron donors should present a significant obstacle to cross-species compatibility, even though the RCs and their respective cytochrome redox carriers share significant structural homology. Here, we investigate the capacity of cyt c_6 and Pc to replace cyt c_2 as the electron donor to RC-LH1 and RC complexes *in silico*, *in vitro* and *in vivo*. We show that cyt c_6 is an adequate replacement for the native cyt c_2 donor *in vivo* despite its intrinsically low RC reduction rate *in vitro*, whilst Pc is a uniformly poor electron donor to RCs in both situations. However, the *in vivo* performance of Pc can be greatly improved by ALE, which has the effect of raising heterologous Pc biosynthesis at least seven-fold. We also identify possible roles for the additional subunits that surround the RC core complex, including the LH1 αβ polypeptides, PufX, protein-Y and protein-Z. Although it is not known which subunits are responsible, the presence of these LH1-associated proteins collectively improves both the activity of the RC complex and its electron donor selectivity.

Results

Cyt c_6 and Pc productively bind RC-LH1 in AlphaFold3 predicted complexes

Once bound together in a complex, the rate of electron transfer between two redox-active proteins is determined by a range of highly sensitive parameters, including the difference in midpoint redox potentials that determines the driving force (ΔG), the reorganisation energy (λ) and the edge-to-edge distance between two redox active cofactors [38]. Whilst RC-donor systems can tolerate significant changes in ΔG values [39], nearly all productive biological electron transfers occur over a narrow distance range of 4–14 Å, making the binding location and orientation of an incoming redox carrier protein functionally imperative [40].

Despite billions of years of divergent evolution, both cyt c_6 and Pc are predicted by AlphaFold3 [41] to bind the *Rba. sphaeroides* RC in the same position as the co-evolved cyt c_2, with their redox-active cofactors positioned less than 14 Å from the special pair in the predicted co-structures (Figure 2). This was also the case for isocytochrome c_2 (iso c_2), a redundant genomically encoded donor to RC-LH1 which is up-regulated in 'spd' suppressor mutants of *Rba. sphaeroides* when the *cycA* gene for cyt c_2 is knocked out [42]. Since the midpoint redox potentials of cyt c_6 (+ 324 mV) and Pc (+ 360 mV) [43] are similar to cyt c_2 (+ 352 mV) [44] and iso c_2 (+ 294 mV) [45], we predicted that all four redox carrier proteins would be capable of reducing P_{865}^+ once bound. The predicted structures also suggest that cyt c_6 and Pc have some
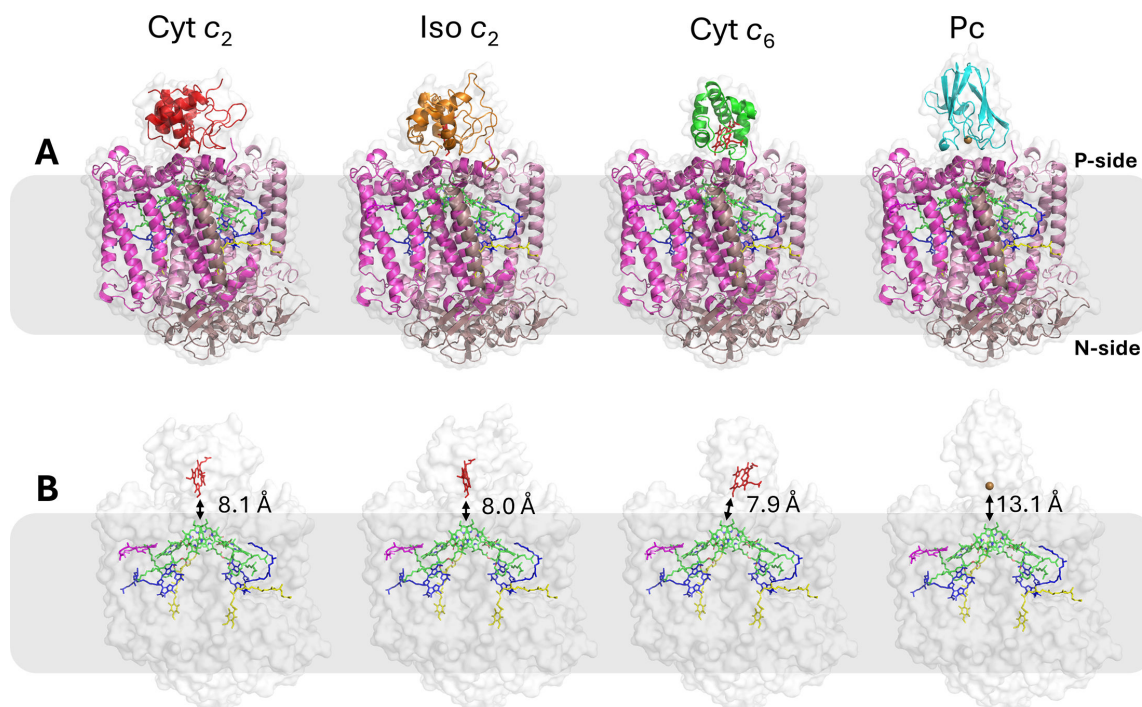
Figure 2: AlphaFold3-predicted complexes of the *Rba. sphaeroides* RC with native and non-native redox carrier proteins.

(**A**) Cartoon representations of the RC-L (pink), RC-M (magenta) and RC-H (brown) core subunits bound to cytochrome c_2 (cyt c_2) (red), isocytochrome c_2 (iso c_2) (orange), cytochrome c_6 (cyt c_6) (green) and plastocyanin (Pc) (cyan). (**B**) Transparent space-filling models of the complexes, with cofactors visible including heme (red), copper (orange), BChl (green), bacteriopheophytin (blue) and UQ (yellow). Distances are labelled, with the predicted edge-to-edge distances between the heme c in cyt c_2 and the primary pair BChls being only slightly lower than the 8.4 Å value determined by X-ray crystallography [20].

affinity for the cyt c_2 binding site on the RC, which is corroborated by protein–protein docking simulations of AlphaFold2-predicted complexes in the HADDOCK 2.4 server [46,47]. In these simulations, the two *Synechocystis* proteins were predicted to make similarly strong vdW interactions with RC-LH1 compared with cyt c_2, but the electrostatic forces were significantly weaker (Supplementary Figure S1), in keeping with their lower surface charge densities (Figure 3). Calculations suggest that the electron transfer rate from Pc is likely to be several orders of magnitude slower than for the cytochromes (Supplementary Table S2), not least because the donor and acceptor cofactors are 13.1 Å apart, the longest of the distances in Figure 2 [20,40,41,43,45,50,51,52].

Both cyt c_6 and Pc can substitute for cyt c_2 *in vivo*

To determine how closely computational predictions correspond to *in vivo* behaviour, a photosynthetically incompetent $\Delta cycA \Delta cycI$ strain of *Rba. sphaeroides* was constructed which lacked both endogenous redox carrier proteins that can support phototrophic growth [42,53]. Plasmid-borne genes encoding the four different electron donor proteins were transferred to the $\Delta cycA \Delta cycI$ strain, generating four transconjugant strains carrying *cycA* (cyt c_2), *cycI* (iso c_2), *petJ* (cyt c_6) or *petE* (Pc). In each transconjugant strain, redox carrier genes were placed under the transcriptional control of a constitutively active promoter, $Ppuf_{843-1200}$, in the broad-host replicative vector pBBRBB [54]. Using a consistent starting inoculum of semi-aerobically grown cells, transconjugants were cultured photoheterotrophically under 24 μmol m^{-2} s^{-1} illumination alongside positive wildtype (WT) and negative $\Delta cycA \Delta cycI$ control strains carrying empty pBBRBB plasmids. The resulting 48-h growth curves and doubling times presented in Figure 4 demonstrate the very similar growth rates of the WT (empty pBBRBB) control and the *cycA* transconjugant strain ($\Delta cycA \Delta cycI::pBBRBB$ *cycA*), whereas the *cycI* (iso c_2) transconjugant strain ($\Delta cycA \Delta cycI::pBBRBB$ *cycI*) grows slightly more slowly, possibly due to the 40-fold lower affinity iso c_2 has for the RC relative to cyt c_2 [55]. The growth curve for $\Delta cycA \Delta cycI::pBBRBB$ *petJ* shows that cyanobacterial cyt c_6 is sufficiently compatible with RC-LH1, cytochrome bc_1 (cyt bc_1) and the host metabolic machinery to restore a near-WT photoheterotrophic growth rate to the *Rba. sphaeroides* $\Delta cycA \Delta cycI$ mutant (Figure 4A). By
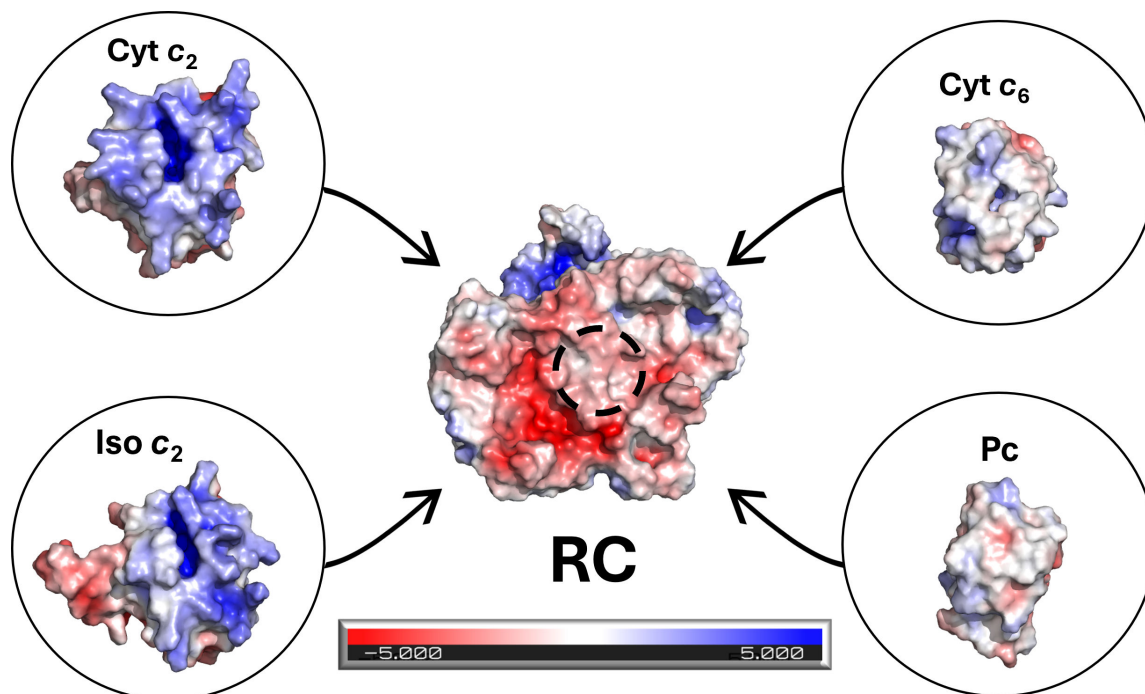
Figure 3: Surface electrostatics of the *Rba. sphaeroides* RC and various soluble electron donors.

Surface charges on the binding faces of selected electron transfer proteins in 'open book' style, showing the periplasmic face of the RC and the incoming faces of the four electron donors (circled) that dock onto the RC. Structures were generated using AlphaFold2 [48], visualised in PyMol and coloured using the APBS plugin [49], with negative charges in red, positive charges in blue and uncharged patches in white, with colour strength denoting charge density. cyt c_2, cytochrome c_2; cyt c_6, cytochrome c_6; iso c_2, isocytochrome c_2; Pc, plastocyanin; RC, reaction centre.

contrast, the *petE* transconjugants were barely viable, with doubling times over 10-fold longer than the WT (Figure 4B). However, after ~10 days of minimal growth, the photoheterotrophic growth rate of the three *petE* transconjugant cultures suddenly increased five-fold (Figure 5A), possibly arising from a growth-enabling suppressor mutation [42,56,57]. This shorter doubling time was maintained when the suppressor strains were isolated and then cultured photoheterotrophically for a second time, with *petE* transconjugants growing only ~3.1 times more slowly than the WT control and without a lag phase (Figure 5A). Relative quantification of redox carrier proteins in the periplasm using sodium deoxycholate (see Materials and methods) revealed that, unlike cyt c_6, the bioavailability of Pc in *petE* transconjugants is initially very poor, and that the mechanistic basis of improved growth is a dramatic improvement in intracellular Pc levels without any changes to the plasmid sequence or knockout loci (Figure 5B). Despite having a mean periplasmic redox carrier concentration 1.7 times higher than in *petJ* transconjugants ($P<0.05$), the fact that the growth rate of the evolved *petE* transconjugants remained almost three-fold slower is further evidence that RC-LH1 and cyt bc_1 are much more compatible with cyt c_6 than Pc under physiological conditions, assuming that all redox carriers are incorporated equally within chromatophore vesicles. Although different methods were used to quantify cytochrome and Pc levels, Figure 5B shows that the amount of Pc accumulated in the periplasm of the evolved *petE* transconjugant strains was twice that of cyt c_2 in the WT strain ($P<0.01$) and over seven times more than the original *petE* transconjugants before ALE occurred ($P<0.001$).

RC-LH1 displays very low compatibility with cyt c_6 and Pc in steady-state turnover assays conducted under low ionic strength

Whilst the behaviour of different redox carriers *in vivo* is a complex function of their affinity for RC-LH1, the cyt bc_1 complex and the host's wider metabolism, *in vitro* steady-state turnover assays allow direct measurement of the compatibility of the four redox carrier proteins with the RC-LH1 complex. Reaction mixtures of 300 μl were made containing a fixed 0.125 μM concentration of RC-LH1, 50 μM UQ-2 (a
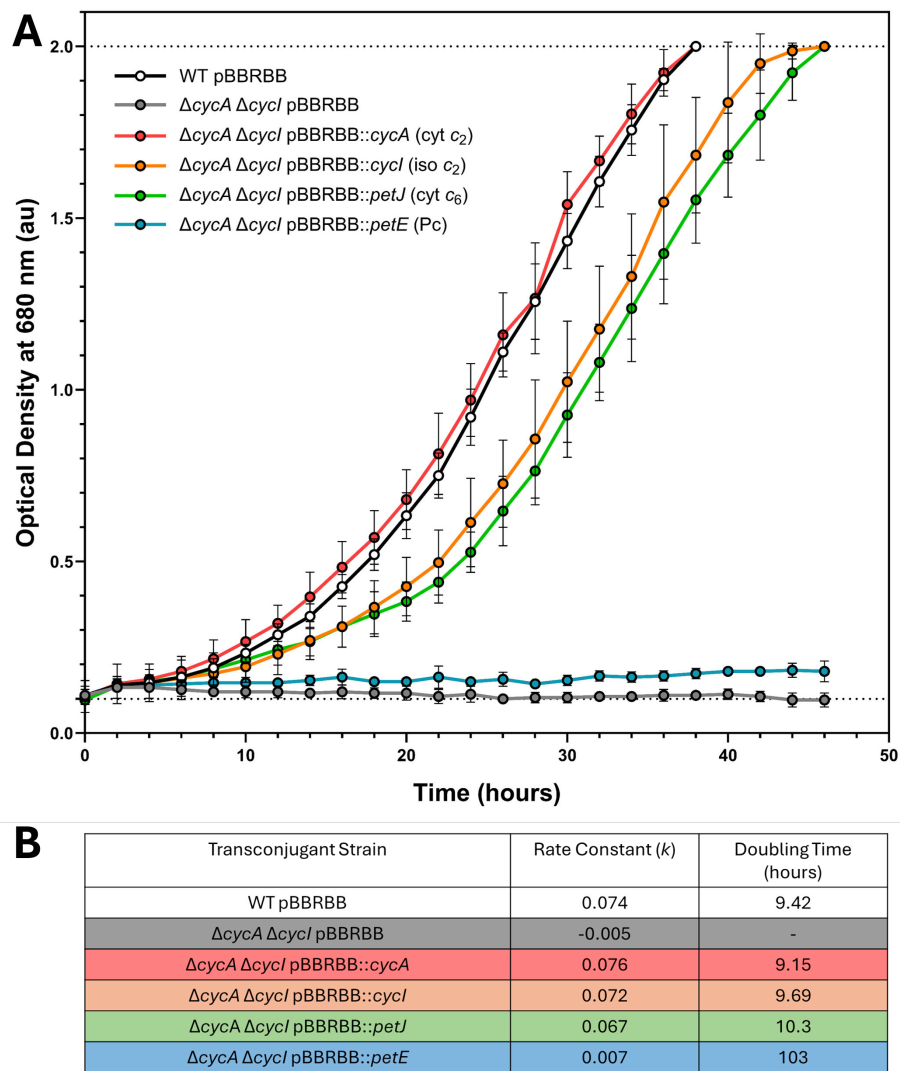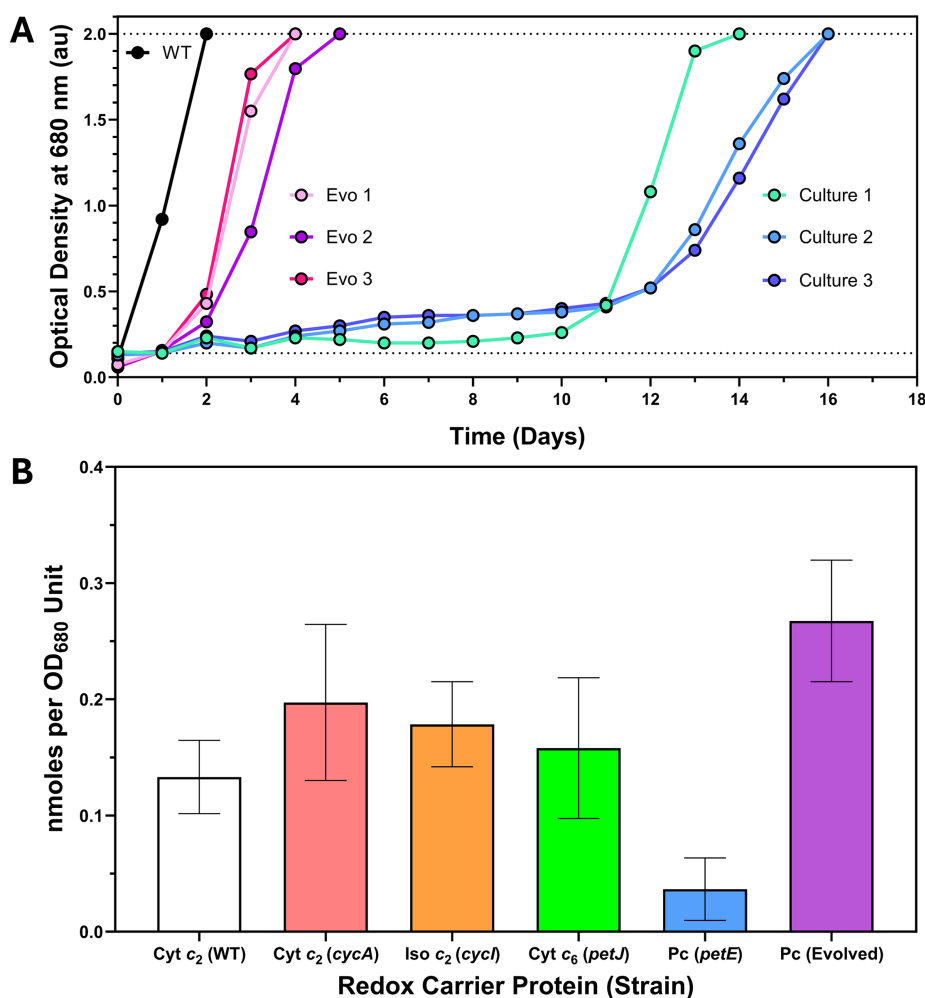
Figure 4: Photoheterotrophic growth curves of *Rba. sphaeroides* strains with native and non-native redox carriers.

(**A**) Cultures were grown in triplicate and measured at 2-h intervals. Dotted lines at Y=0.1 and Y=2 represent the starting OD_{680} values and detection limit, respectively. (**B**) Table of growth rate parameters colour coded according to the data in panel (**A**). In panel (**A**) and all subsequent instances, the error bars displayed are +/−1 standard deviation from the mean and n=3 unless otherwise stated.

soluble analogue of the native UQ-10 substrate with a shorter isoprenoid tail) and a ≥20-fold molar excess of one of the pre-reduced redox carrier proteins, each of which was purified from the periplasm using a novel technique involving sodium deoxycholate (see Materials and methods). In each assay, RC turnover was initiated by continuous illumination with an 810 nm light-emitting diode (LED) and the oxidation of reduced donors monitored by measuring absorbance at their respective redox-sensitive wavelengths. These reactions were conducted in triplicate under the optimum *in vitro* conditions for the RC-LH1-cyt c_2 system (50 mM Tris-HCl at pH 7.5 with 100 mM NaCl and 0.03% (w/v) n-dodecyl-β-D-maltoside (β-DDM)) as determined by separate steady-state turnover experiments (see next section and Supplementary Figure S2). To act as a benchmark for turnover rates, the performance of cytochrome *c* (cyt *c*) from horse heart mitochondria was also measured, since this commercially available protein has been used extensively as an effective *in vitro* analogue of cyt c_2 in historical RC literature despite sharing just 32.7% sequence identity [58,59]. A titration series was conducted for each redox carrier protein and the initial rates of oxidation used to construct Michaelis–Menten plots, from which V_{max} and K_M values could be calculated (Figure 6).

The Michaelis–Menten plots in Figure 6A–C display a clear disparity between the native redox carrier proteins from *Rba. sphaeroides* and their counterparts from *Synechocystis*, with a compatibility

Figure 5: Photoheterotrophic growth curves of *petE* transconjugants and relative periplasmic concentrations of redox carrier proteins in all transconjugant strains.

(**A**) Extended photoheterotrophic growth curves comparing WT pBBRBB (positive control, black) to individual *petE* transconjugant cultures (genotype Δ*cycA* Δ*cycI* pBBRBB::*petE*, blue shades). Cells from each *petE* culture were harvested, streaked to single colonies on M22 agar and grown semi-aerobically to make three evolved strains (Evo 1, Evo 2 and Evo 3), with each number corresponding to the culture number from which the cells were isolated. These Evo strains were then grown photoheterotrophically under the same conditions as the original set of growth curves, with the resulting data superimposed onto the 16-day growth curves (pink shades). The average doubling time of the evolved *petE* transconjugants in the second growth experiment was 28.6 h with a rate constant of 0.0243, approximately five times faster than in the first growth experiment. (**B**) The relative amounts of each redox carrier protein that could be extracted from the periplasm of each transconjugant strain using sodium deoxycholate (see Materials and methods). Three biological replicates were conducted for all proteins, except for Pc in the evolved strains (purple), for which $n=9$. cyt c_2, cytochrome c_2; cyt c_6, cytochrome c_6; iso c_2, isocytochrome c_2; Pc, plastocyanin.
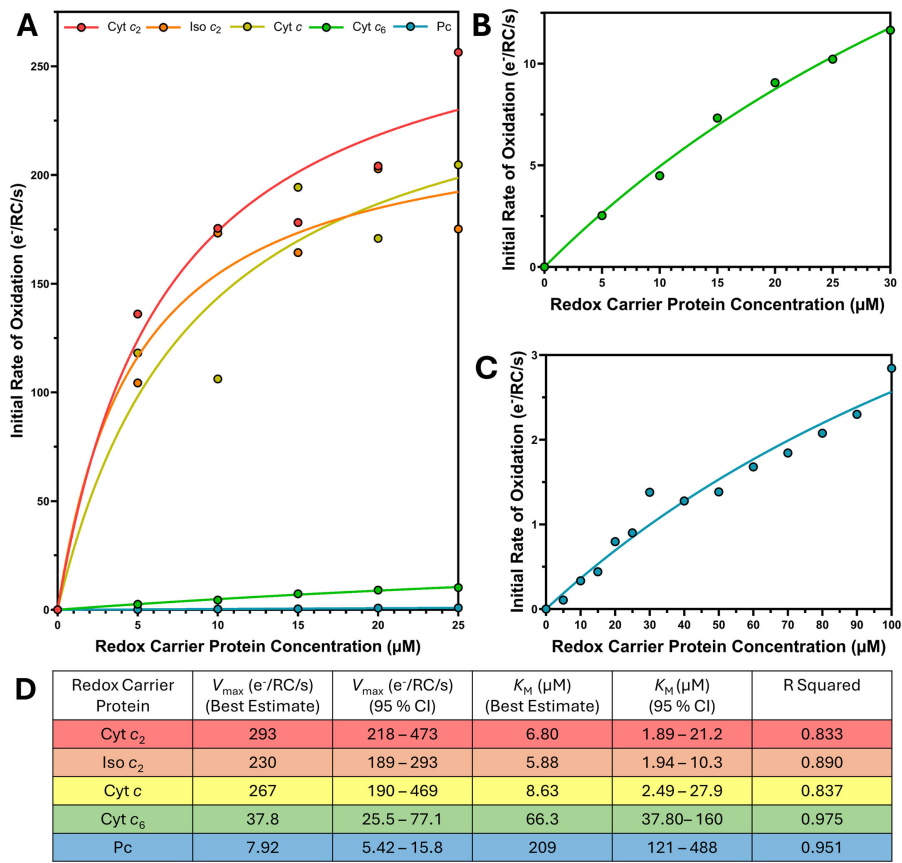
order matching the *in vivo* growth curves and the HADDOCK 2.4 predicted affinities. Under the assay conditions, there was little difference in the V_{max} and K_M values for cyt c_2, iso c_2 and cyt c, which all lie within error of each other, but the oxidation rates of cyt c_6 and Pc were much slower than the *in vivo* results would suggest (Figure 6D). This indicates that whilst cyt c_6 and Pc can reduce P_{865}^+ fast enough *in vivo* to support photoheterotrophic growth, their intrinsic level of compatibility with the RC-LH1 complex is very low outside the confined chromatophore environment.

Redox carrier proteins from *Rba. sphaeroides* and *Synechocystis* display opposite salinity trends in their interactions with RC-LH1

Whilst there is a clear oxidation rate hierarchy for the different redox carriers, the conditions used to collect the data in Figure 6 are unlikely to reflect the physiological conditions within chromatophores and may selectively favour the oxidation of the two native redox carriers by RC-LH1. To determine the optimum
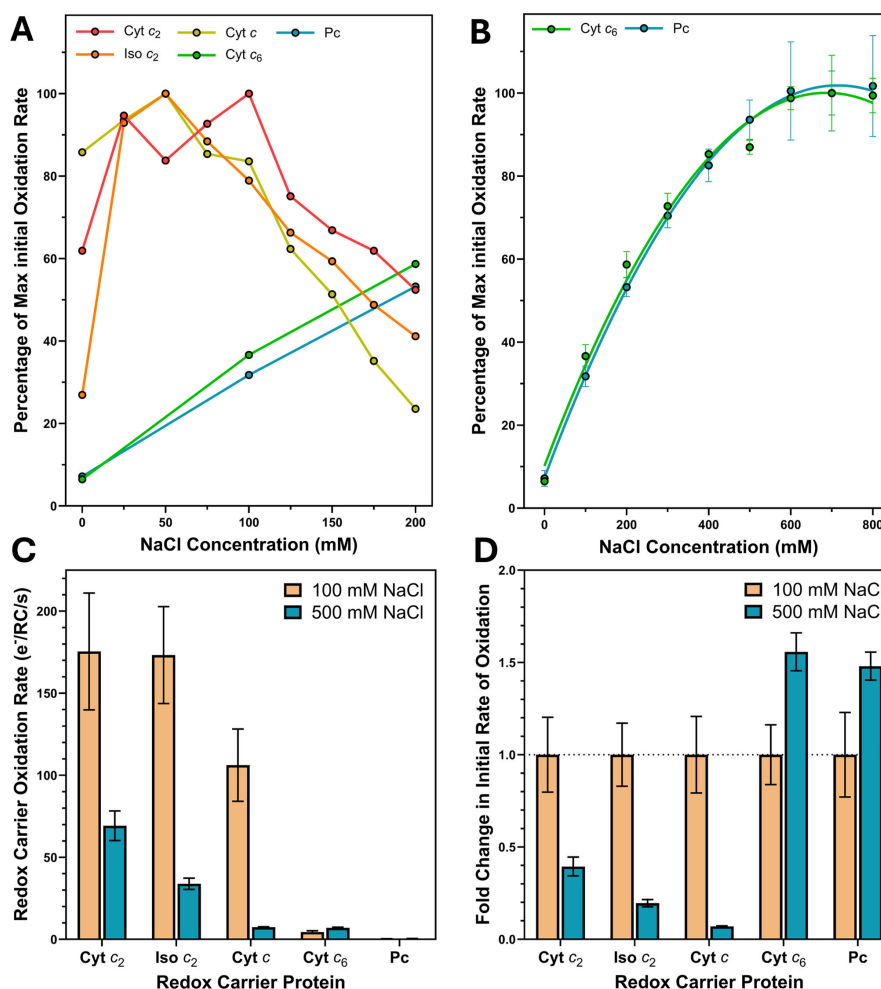
NaCl concentrations for the oxidation of the five different redox carrier proteins by RC-LH1, steady-state turnover assays were conducted at pH 7.5 with 0.25 µM RC-LH1 and a fixed 80-fold excess of redox carrier protein, along with 50 µM UQ-2, 0.03% (w/v) β-DDM and 1 mM ascorbate for cyt c_2, iso c_2 and cyt c, with NaCl added at 25 or 100 mM intervals.

Plotting oxidation rate against salinity, as shown in Figure 7A and B, reveals decidedly different behavioural trends between the two groups of redox carrier proteins with RC-LH1; whilst the oxidation rates of cyt c_2, iso c_2 and cyt c are highest between 25 and 100 mM NaCl, the optimum NaCl concentrations for cyt c_6 and Pc are much higher, lying between 600 and 800 mM. These dramatically increased, and nearly identical, optimum salt concentrations for cyt c_6 and Pc may be a consequence of incompatible electrostatic interactions with RC-LH1 that are screened at high salinities. Amongst the three redox carrier proteins that perform better under lower salinities, it is perhaps unsurprising that the physiological RC-LH1 electron donor, cyt c_2, has both the highest optimum NaCl concentration and is the least affected by salt-screening, with the RC-LH1-cyt c_2 system retaining about 40% of its maximum activity at 500 mM NaCl (Figure 7C). By contrast, the interaction between RC-LH1 and cyt c is more easily disrupted by salinity, having lost 90% of its cyt c oxidation activity by 500 mM (Figure 7C), with an observed 50 mM optimum NaCl concentration comparable with the 40-mM value found previously for the antenna-free RC-cyt c system (Figure 7A) [59]. The decline in iso c_2 oxidation rate is intermediate between cyt c_2 and cyt c, with only 20% of maximum activity remaining at 500 mM, revealing a clear order of electrostatic

D	Redox Carrier Protein	V_{max} (e⁻/RC/s) (Best Estimate)	V_{max} (e⁻/RC/s) (95 % CI)	K_M (µM) (Best Estimate)	K_M (µM) (95 % CI)	R Squared
	Cyt c_2	293	218 – 473	6.80	1.89 – 21.2	0.833
	Iso c_2	230	189 – 293	5.88	1.94 – 10.3	0.890
	Cyt c	267	190 – 469	8.63	2.49 – 27.9	0.837
	Cyt c_6	37.8	25.5 – 77.1	66.3	37.80 – 160	0.975
	Pc	7.92	5.42 – 15.8	209	121 – 488	0.951

Figure 6: Michaelis–Menten plots, including V_{max} and K_M estimates for oxidation of different redox carriers by RC-LH1 complexes.

(**A**) Michaelis–Menten plots of redox carrier oxidation rate at 25℃ against the concentration of cyt c_2 (red), iso c_2 (orange), cyt c (yellow), cyt c_6 (green) and Pc (blue). (**B**) Expanded Michaelis–Menten plot of redox carrier oxidation rate versus cyt c_6 concentration. (**C**) Expanded Michaelis–Menten plot of redox carrier oxidation rate versus Pc concentration. (**D**) Estimates for V_{max} and K_M, along with the 95% confidence intervals for both parameters and the coefficient of determination (R-squared) demonstrating the goodness of fit to the Michaelis–Menten equation used to determine the two parameters in GraphPad Prism 10 (Domatics). 1 mM ascorbate was included in the reaction mixtures of cyt c_2, iso c_2 and cyt c to keep each donor reduced before the light-on time. However, this reagent was omitted from reaction mixtures containing cyt c_6 or Pc as these proteins remained reduced during dark adaption and ascorbate addition was found to lower their oxidation rates and amplitudes. cyt c, cytochrome c; cyt c_2, cytochrome c_2; cyt c_6, cytochrome c_6; iso c_2, isocytochrome c_2; Pc, plastocyanin.

Figure 7: Effect of increasing NaCl concentration on initial rates of redox carrier oxidation by RC-LH1 complexes.

Salt dependency of the interactions between RC-LH1 with (**A**) all redox carriers between 0 and 200 mM NaCl and (**B**) Pc and cyt c_6 between 0 and 800 mM NaCl. All reactions were carried out in triplicate and normalised to the maximum rate for each redox carrier, thus the graphs show the percentage change in activity with increasing salinity. Error bars are omitted from panel (**A**) for ease of viewing, with just the mean values plotted for each salt concentration, whilst in panel (**B**), the data are fitted to a centred second-order polynomial (quadratic) function, with R-squared values of 0.98 for both cyt c_6 and Pc. (**C**) Raw initial rates of redox carrier oxidation by RC-LH1 under low salinity (100 mM NaCl, orange) and high salinity (500 mM NaCl, blue). (**D**) Fold change in initial rates of redox carrier oxidation by RC-LH1 from 100 mM (orange) to 500 mM NaCl (blue). All reactions were carried out at 25℃, with each 300 µl reaction mixture containing 0.25 µM RC-LH1, 10 µM redox carrier protein, 50 µM UQ-2, 50 mM Tris-HCl at pH 7.5 and 1 mM ascorbate for cyt c_2, iso c_2 and cyt c. (**A**) Raw oxidation rates for the data in panels (**A**) and (**B**) can be found in Supplementary Figure S3. cyt c, cytochrome c; cyt c_2, cytochrome c_2; cyt c_6, cytochrome c_6; iso c_2, isocytochrome c_2; Pc, plastocyanin.

complementarity, where cyt c_2 makes the most specific and high-affinity interactions with RC-LH1. A consequence of this differential salt dependency is that at much higher salt concentrations, the gap in RC-LH1 reduction activity between the native and *Synechocystis* redox carriers is significantly lower (Figure 7C), although the compatibility of Pc remains poor.

LH1 ring subunits modulate both acceptor and donor side electron transfer activity

Since the first RC purification by Reed and Clayton in 1968 [60], it has been a common practice to solubilise *Rba. sphaeroides* membranes in detergents such as Triton X-100 or lauryldimethylamine oxide (LDAO) which removes LH1-associated subunits (mainly LH1 α, β, as well as X, Y and Z), leaving behind the more experimentally accessible RC-only complex. In steady-state turnover assays, this truncated complex, which consists of just the three core RC L, M and H subunits, behaves very differently to the physiological RC-LH1 system under its optimal conditions (50 mM Tris at pH 7.5, 100 mM NaCl). Not
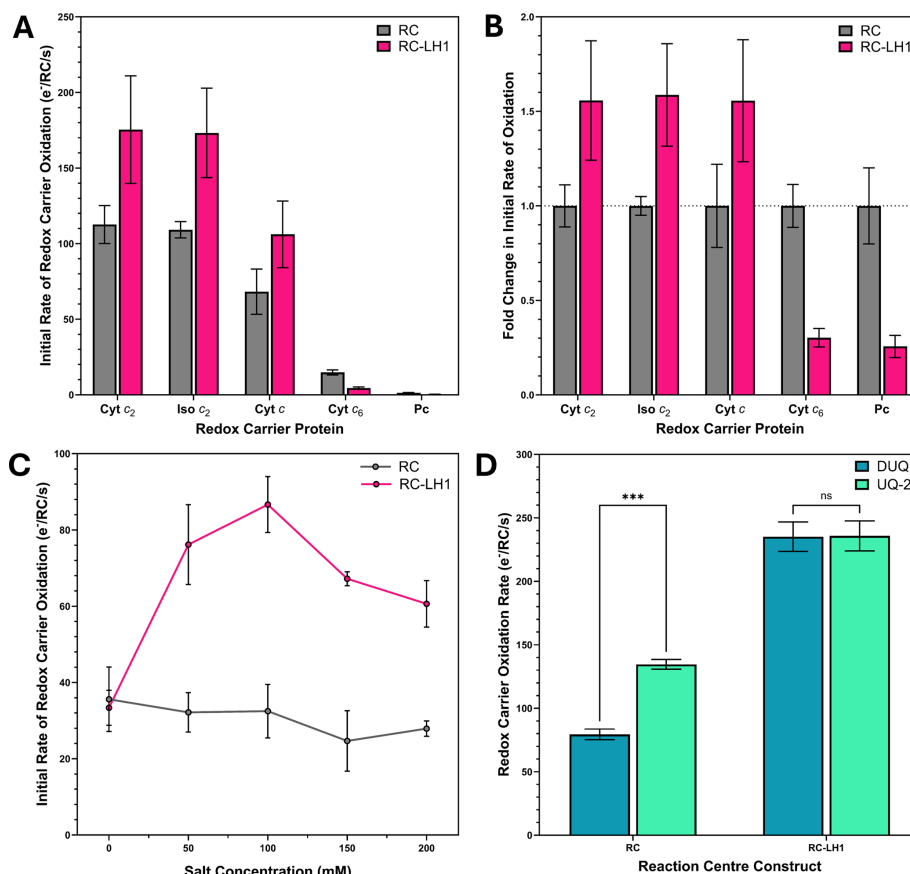
Figure 8: Kinetic behaviour of RC-only and RC-LH1 complexes under different conditions.

(**A**) Raw initial rates of redox carrier oxidation during steady-state turnover assays by RC-LH1 (pink) and RC-only complexes (grey). Assays were conducted at 25°C in 50 mM Tris-HCl pH 7.5 and 0.03% (w/v) β-DDM, with 0.125 μM RC or RC-LH1, 10 μM redox carrier, 50 μM UQ-2 and 1 mM sodium D-ascorbate. (**B**) Fold change in RC-LH1 initial oxidation rates compared with RC-only for each redox carrier protein, from the dataset plotted in (**A**). (**C**) Initial rates of cyt c_2 oxidation by RC-LH1 (pink) and RC-only complexes (grey) in response to increasing [NaCl], with conditions of 0.5 μM RC/RC-LH1, 10 μM cyt c_2 and 0.03% (w/v) β-DDM in 50 mM Tris-HCl pH 8, along with 1 mM ascorbate for reaction mixtures containing RC-LH1 but not RC-only complexes. (**D**) Bar chart comparison of initial rates of cyt c_2 oxidation by RC-LH1 and RC-only complexes with two different quinone analogues, decylubiquinone (DUQ, blue) and UQ-2 (cyan). Reactions were carried out with 0.5 μM RC/RC-LH1, 11 μM cyt c_2, 0.5 mM ascorbate and 50 μM DUQ/UQ-2, with a *P* value of <0.001 (***) for the RC-only complex with the two different analogues, calculated from an unpaired *t*-test using the Holm–Šídák method to account for multiple comparisons. cyt *c*, cytochrome *c*; cyt c_2, cytochrome c_2; cyt c_6, cytochrome c_6; iso c_2, isocytochrome c_2; Pc, plastocyanin.

only is the cyt c_2 oxidation rate by the RC-only complex more than 30% slower than that by RC-LH1 (Figure 8A and B), but it also appears to be salt concentration independent under the conditions of this steady-state assay (Figure 8C). Since only the solvent-exposed cyt c_2-binding site (donor side) of the complex is affected by salt, this result suggests that the activity of the RC-only complex is held back by Q$_B$ turnover, making it acceptor side limited. This theory is corroborated by an observed increase in cyt c_2 oxidation rate by RC-only complexes when decylubiquinone (DUQ) was exchanged for UQ-2, a UQ analogue with a more physiological tail composed of two isoprene units rather than a saturated decane chain, whilst no difference in behaviour was observed between these two analogues with RC-LH1 (Figure 8D). This phenotype was found to be highly robust and repeatable, being observed consistently across many technical and biological repeats, including when RC-only complexes were purified from LH1-minus Δ*pufBA* strains or directly from photoheterotrophically grown RC-LH1 complexes containing spheroidene by LDAO treatment (data not shown). Follow-up steady-state turnover experiments also confirmed that this difference in quinone analogue sensitivity between the two forms of the RC complex cannot be explained by the additional light-harvesting capacity of the LH1 ring, since under the conditions of the assay, the RC-only complex is already light-saturated (Supplementary Figure S4).

Along with responding differently to salinity, cyt c_6 and Pc also display opposite trends to cyt c_2 with the truncated RC-only complex (Figure 8A and B). Whilst the initial oxidation rates of cyt c_2, iso c_2 and

cyt c are all improved ~1.5-fold by switching from the RC-only to the RC-LH1 version of the complex, the opposite is true for cyt c_6 and Pc, whose oxidation rates drop three-fold. This suggests that there is a fundamental incompatibility between the *Synechocystis* redox carrier proteins and the LH1-associated subunits that surround the RC core complex. Collectively, these subunits appear to not only confer higher acceptor side activity by improving quinone reduction but also seem to impart greater donor side selectivity by hindering the binding of non-cognate proteins that lack the correct properties. The LH1 ring may also promote cyt c_2 binding through electrostatic steering, as suggested in our recent single molecule force spectroscopy study [28], which could also contribute to the observed difference in cyt c_2 oxidation rates between RC-only and RC-LH1 complexes.

Discussion

The data presented in the present study demonstrate that despite billions of years of divergent evolution, the *Rba. sphaeroides* RC-LH1 complex displays a surprisingly high level of *in vivo* compatibility with the cyanobacterial cyt c_6 and Pc redox carriers from *Synechocystis* sp. PCC 6803, which usually reduce PSI. Although both *Synechocystis* proteins can shuttle electrons between the RC-LH1 and cyt bc_1 complexes efficiently enough to support photoheterotrophic growth *in vivo*, *in vitro* and *in silico* data paint a more complex picture of compatibility compared with the two native redox carrier proteins in *Rba. sphaeroides*. Computational modelling predictions, photoheterotrophic growth rates and steady-state turnover assays all converge on a predicted RC-LH1 compatibility order where cyt c_2 is the best electron donor to P_{865}, followed by iso c_2, then cyt c_6 and finally Pc, but different methods give different relative estimates due to fundamental differences in behaviour between these redox carrier proteins. Whilst cyt c_2 and iso c_2 were oxidised fastest by RC-LH1 at low salinities (50–100 mM NaCl), the highest turnover rates for cyt c_6 and Pc were achieved with the RC-only complex and high salinities (600–750 mM). A third non-native redox carrier, cyt c from *Equus caballus*, showed the same trends as the *Rba. sphaeroides* redox carriers, but its performance compared with the native *Rba. sphaeroides* cyt c_2 fell away sharply with increased salinity. Taking all these data together, several key differences emerge between the RC-LH1-cyt c_2 and PSI-cyt c_6/Pc systems, as well as some unexpected properties of the RC-LH1 complex. Although Pc is intrinsically much less compatible with RC-LH1, likely because it hails from a different family of proteins, the identical behavioural trends exhibited by cyt c_6 and Pc are in keeping with their isofunctional roles in thylakoid electron transfer [61,62]. Regardless of the nature of their interaction, it may be that any reduced electron carrier protein with a suitable redox potential can reduce P_{865}^+ if its redox-active cofactor can be positioned within 14 Å of the special pair.

The rate at which different redox carrier proteins can reduce the RC-LH1 complex in the steady state is a function of three countervailing processes, binding (k_{on}), electron transfer (k_{ET}) and unbinding (k_{off}), all of which require a range of different parameters to be maintained within a narrow range. Protein–protein docking in AlphaFold3 and HADDOCK 2.4 suggests that both cyt c_6 and Pc bind RC-LH1 in sufficient proximity and in the correct orientation to support productive electron transfer (Figure 2) (Supplementary Figure S1), but their different surface properties are a barrier for binding to the RC (Figure 3). Whilst both long-range electrostatic steering and short-range hydrophobic interactions are important for binding both PSI and RC-LH1, the binding partners in *Rba. sphaeroides* have a much greater electrostatic force component, whilst cyt c_6 and Pc have much lower surface charge densities (Figure 3). As a result of these differences, it may be that the PSI cyt c_6/Pc binding interface is intrinsically weaker than RC-LH1-cyt c_2/iso c_2, especially since the experimentally determined K_D for plant PSI-Pc [63] is 70 times greater than RC-cyt c_2 [64].

Very low oxidation rates were measured for cyt c_6 and Pc with RC-LH1 in the 50-150 mM NaCl range that favours the native cyt c_2 electron donor, but were greatly improved at high salinities in the 500-800 mM range (Figure 7). The binding faces of cyt c_6 and Pc are not highly charged, unlike cyt c_2 (Figure 3), but the highly negatively charged surface of the RC-LH1 complex (Figure 9A) could present a significant barrier to forming initial encounter complexes with cyt c_6 and Pc, especially if unproductive electrostatic interactions are occurring between the RC-LH1 complex and the non-binding faces of cyt c_6 and Pc. We suggest that high salinities mask these incompatibilities and this could also explain why cyt c_6 and Pc oxidation rates improve when the highly charged LH1 ring is removed from the complex.

Taken together, the differential effects of salt screening and subunit composition on the redox carrier proteins also suggest that the subunits that surround the RC core complex are required not only for light harvesting but also for maximising the activity and selectivity of electron donors under optimal conditions.

If the surface charges on each LH1 αβ pair can be unfavourable for the binding of cyt c_6 and Pc, then it is likely that the opposite can be true for the native RC-LH1 electron donor, with molecular dynamics data suggesting that the LH1 ring has a degree of affinity for cyt c_2 [28]. It is, therefore, possible that LH1 αβ pair electrostatics are partially responsible for the observed rate difference in cyt c_2 oxidation between RC-only and RC-LH1 complexes, with possible roles for surface charges in recruitment, orientation, and entrance and exit pathways for redox carrier proteins (Figure 9B). However, this difference can also be explained by an acceptor side limitation in the truncated three-subunit RC-only complex, which is supported by the sensitivity of its turnover rate to different quinone analogues. The way that RC-LH1 complexes are donor-side limited under the same conditions and do not respond to quinone analogue changes suggests the LH1 α and β polypeptides that surround the RC, along with the X, Y and Z subunits, act in concert to increase acceptor side quinone turnover. The mechanism by which these subunits enhance acceptor side turnover could involve providing efficient entrance and exit channels, providing a 'conveyor belt' pathway for quinones to rapidly enter the Q_B binding site and leave as soon as they are doubly reduced [65,66]. Additional low-affinity UQ binding sites, which might act as a 'waiting room' to increase the local concentration of incoming quinones, have already been identified in cryo-EM structures of the *Rhodopseudomonas palustris* RC-LH1 complex and involve π-stacking interactions between tryptophan residues and quinone head groups [65,67], whilst π-stacking and hydrogen bonding with side chains on LH1 αβ subunits have also been implicated in quinol exit pathways [66]. In the *Rba. sphaeroides* RC-LH1 complex, accessory entrance and exit sites might be found in the transmembrane helices of the αβ pairs, or might even be associated with the X, Y and Z subunits which are already known to maintain open quinone channels to the membrane, completing a 'highway' for quinone diffusion between RC-LH1 and cyt bc_1 [53,67–71].

Ultimately, however, under almost all light levels, the activity of the RC-LH1 complex is not limiting for photosynthetic growth; the slowest step in the cyclic purple bacterial electron transport chain is widely acknowledged to be quinol oxidation by the cyt bc_1 complex instead [72–74]. This means that a non-native redox carrier protein substituting for cyt c_2 would not limit photosynthetic growth rate if it oxidised cyt bc_1 and reduced RC-LH1 more rapidly than the cyt bc_1 complex can oxidise ubiquinol. For *petJ* and *petE* transconjugant strains growing photoheterotrophically (Figure 4), a slower rate of RC-LH1 re-reduction could be tolerated with only a slight increase in doubling time, masking the true difference in compatibility between the native redox carrier proteins and their counterparts from *Synechocystis*. This could explain why, following ALE of *petE* transconjugants by a currently unknown mechanism, the compatibility of cyt c_6 and Pc unusually appears higher *in vivo* than *in vitro*, rather than the other way around.

The differences between *in vivo* and *in vitro* data summarised in Table 1 can also be reconciled in the context of the conditions of the chromatophore lumen, which will almost certainly have a pH, viscosity and salinity that differ from laboratory conditions whilst also containing different types of salts and solutes, plus a lipid bilayer. The conditions inside a chromatophore vesicle cannot be replicated *in vitro* and in
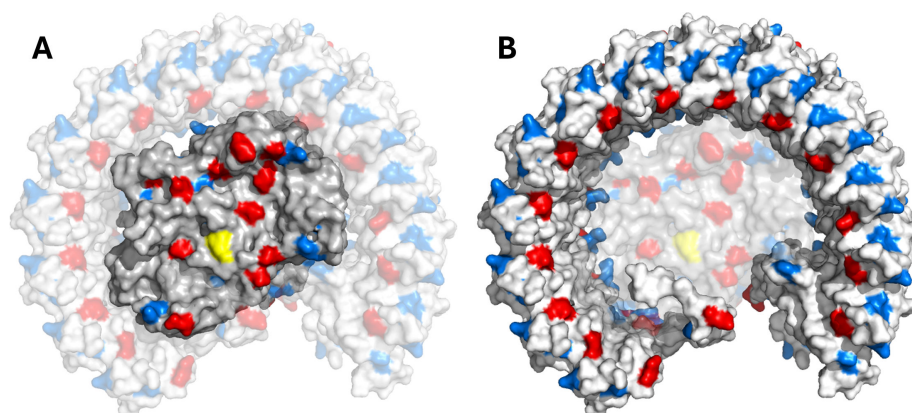
Figure 9: Comparison of surface electrostatics on the periplasmic faces of the RC and LH1 components of the RC-LH1 complex.

(**A**) Surface representation of the periplasmic faces of the RC-L and RC-M subunits with other subunits set to 65% transparency, whilst (**B**) shows the periplasmic face of the rest of the complex, including all ring subunits (α, β, X, Y and Z chains), with RC-L and RC-M set to 65% transparency. In both (**A**) and (**B**), amino acids with negatively charged side chains are coloured red, with positively charged residues in blue and Tyr-L162 shown in yellow to mark the site of electron transfer. Structure shown in this figure is the RC-LH1 monomer complex from [16], PDB 7PIL.

Table 1: Summary of experiments conducted with host and *Synechocystis* redox carrier proteins

	Cyt c_2	Iso c_2	Cyt c_6	Pc
Edge-to-edge distance (Å)	8.1	8.0	7.9	13.1
HADDOCK Score	−183	−144	−104	−91.9
Predicted k_{et} (s^{-1})	1.38×10^9	7.53×10^9	3.23×10^9	2.77×10^5
Doubling time (hours)	9.15	9.69	10.3	36.1
V_{max} (e$^-$/RC/s)	293	230	37.8	7.92
K_M (µM)	6.80	5.88	66.3	209
Optimum [NaCl] (mM)	100	50	700	700

Cyt c_2, cytochrome c_2. Cyt c_6, cytochrome c_6. Iso c_2, isocytochrome c_2. Pc, plastocyanin.

this tiny compartment, which has a typical internal diameter of just 45 nm [75], K_D and K_M values are rendered irrelevant by the effective redox carrier concentration within the chromatophore lumen, which for cyt c_2 is estimated to be 600 µM [73], a value of 3 orders of magnitude greater than the K_D value of 0.3 µM for the RC-cyt c_2 system [64]. The periplasmic concentrations for cyt c_6 and Pc in the ALE strains are comparable to that for cyt c_2 (Figure 5B) and, therefore, still exceed the measured K_M values of 66 and 209 µM, respectively. Thus, *in vivo* compartmentalisation of reactants can overcome apparent *in vitro* limitations, and in this case, excess amounts of cyt c_6 and Pc are already capable of productively shuttling electrons between RC-LH1 and cyt bc_1, raising the prospects that synthetic biology can bring together photosynthetic proteins that evolution has long since separated.

Materials & methods

Generation of strains and plasmids

The work described in the present study was carried out in several strains of *Rba. sphaeroides* 2.4.1, along with *E. coli* strains for molecular cloning and conjugative transfer of plasmids, all of which are listed in Table 2. For complementation studies and protein production, an unmarked genomic deletion strain lacking the endogenous photosynthetic redox carrier genes (genotype Δ*cycA* Δ*cycI*) was generated using the pK18mob*sacB* system as previously described [53]. The DX13 and E9 strains lacking various RC-LH1 and LH2 genes were generated by sequential rounds of pK18mob*sacB* mutagenesis following the protocol detailed in [79]. Unmodified genes encoding cyt c_2 (*cycA*), iso c_2 (*cycI*), cyt c_6 (*petJ*) and Pc (*petE*) were PCR-amplified from their host organism using primers listed in Supplementary Table S1, digested with BglII and XhoI/SalI (Thermo Fisher Scientific), then ligated into the broad-host range vector pBBRBBB-*Ppuf*$_{843-1200}$ [54]. Following sequence verification (Eurofins Genomics), the resulting plasmids were transformed into *E. coli* S17-1 and conjugated into the Δ*cycA* Δ*cycI* strain of *Rba. sphaeroides*, using 30 µg ml^{-1} kanamycin to select transconjugants. A similar strategy was employed for the RC subunit-encoding *pufLM* genes, with PCR fragments being cloned into the same vector at the BglII/SpeI restriction sites, and conjugation of the ligated plasmid into the E9 (Δ*puc1BA* Δ*pufBALM*) strain. A *petE*-StrepII-tag insert was also made by PCR from *Synechocystis* sp. PCC 6803 cells are cloned into a pET28a vector using NcoI and XhoI restriction sites, then transformed into the *E. coli* BL21(DE3) strain (Promega) for Strep-tagged Pc production.

Semi-aerobic growth of *Rba. sphaeroides* cells

Rba. sphaeroides cells were cultured in M22+ medium [80]. Kanamycin (30 µg ml^{-1}) was added to maintain plasmids where necessary. Three different types of flat-bottomed glassware were used to make liquid cultures. In the first liquid culture step, universal tubes containing 10 ml of medium (about 25% full) were inoculated with single colonies from M22 agar plates and grown at 30°C with shaking at 150 rpm until pigmented (~24–48 h). A single 10 ml culture was then used to inoculate either 80 ml medium in a 125-ml Erlenmeyer flask and grown overnight, or 1.6 L medium in a 2-L conical flask and grown for 72 h. The universal tubes were sealed with a screw top cap; the other cultures were kept sterile with a cotton wool bung topped with two layers of aluminium foil.

Photoheterotrophic growth of *Rba. sphaeroides* cells

Anoxic conditions promoting photoheterotrophic growth were achieved by fully filling and stoppering glassware with M22+medium. Larger cultures for RC-LH1 purification were grown in 1-l Roux bottles stoppered with a rubber bung, whilst for growth curves, narrow ~18-ml glass Hungate tubes were inoculated with cells from semi-aerobic 80-ml cultures, using the OD_{680} value to estimate culture turbidity and calculate the amount of inoculum needed to ensure a consistent starting cell density of ~0.1. Cultures were illuminated by a 70-W Halogen Classic Bulbs (Phillips) usually at 25 μmol photons m^{-2} s^{-1} and agitated with magnetic stirrers until reaching stationary phase, which corresponds to an approximate OD_{680} of 3. Growth curve culture turbidity at 680 nm was measured with a C07500 Colorwave colorimeter (WPA). The doubling times of photoheterotrophic cultures were calculated by non-linear fitting in GraphPad Prism 10 using the exponential (Malthusian) growth function.

Purification of intracytoplasmic membranes

All RC-LH1 complexes were purified as monomers from DX13 cells (Δ*puc1BA* Δ*puc2BA* PufX R49L R53L) grown photoheterotrophically in a 1-L Roux culture bottle as described above. Cells were harvested at 4200×*g* for 30 min at 4°C, and the resulting pellets were resuspended in 50 mM Tris-HCl pH 8 supplemented with an EDTA-free protease inhibitor tablet (Merck) to a total volume of 30 ml. Resuspended cells were incubated at room temperature with lysozyme for 20 min, before DNase I was added and the cells were placed on ice. Cells were lysed by two passages through a chilled French press at 124 MPa, and the lysate was clarified by centrifugation at 27,000×*g* for 20 min at 4°C to remove cell debris. Intracytoplasmic membranes (ICM) were prepared by layering clarified supernatant on top of a 15/40% (w/v) discontinuous sucrose gradient, then centrifuged at 84,500×*g* for 10 h at 4°C. The pigmented band of

Table 2: Bacterial strains used in the present study

Species/strain	Genotype	Properties	Source/reference
***Rhodobacter sphaeroides* 2.4.1**			
WT	N/A	WT strain	S. Kaplan (University of Texas)
Δ*cycA* Δ*cycI*	Δ*cycA* Δ*cycI*	Unmarked deletion of *cycA* (RSP_0296) and *cycI* (RSP_2577); does not produce cyt c_2 (*cycA*) or iso c_2 (*cycI*)	[53]
DX13	Δ*puc1BA* Δ*puc2BA* PufX R49L R53L	Unmarked deletion strain of LH2 genes, *puc1BA* (RSP_0314–0315) and *puc2BA* (RSP_1556–1557). Replacement of arginine residues in PufX responsible for dimerisation with leucine so the strain exclusively makes RC-LH1 monomers	This study; S. Kaplan (University of Texas) (Δ*puc1BA*) [76] (Δ*puc2BA*) [77] (PufX R49L R53L)
E9	Δ*puc1BA* Δ*pufBALM*	Unmarked deletion strain of LH2 genes, *puc1BA* (RSP_0314–0315), along with *pufBALM* (RSP_6108, RSP_0258–0256) encoding the RC-LH1 L, M, α and β subunits	This study; S. Kaplan (University of Texas) (Δ*puc1BA*)
Escherichia coli			
Bl21(DE3)	F−*ompT hsd*SB ($r_B^−$, $m_B^−$) *gal dcm* (DE3)	Protein production strain	Promega
JM109	*end*A1, *rec*A1, *gyr*A96, *thi*, *hsd*R17 ($r_k^−$, m_k^+), *rel*A1, *sup*E44, Δ(*lac-proAB*), [F′ *tra*D36, *pro*AB, *laqI*ᑫZΔM15]	Cloning strain	Promega
S17-1	RP4-2 (Tc::Mu, Nm::Tm7) integrated into the chromosome Tp^R Sm^R *rec*A, *thi*, *pro*, *hsd*M⁺	Conjugative transfer of plasmids to *Rba. sphaeroides*	[78]
***Synechocystis* sp. PCC 6803**			
WT	N/A	Glucose-tolerant WT strain	R. Sobotka (Algatech, Třeboň)

WT, wildtype.

ICM formed at the interface was harvested with a serological pipette and centrifuged again at 185,500×g for 2 h at 4°C.

Purification of RC-LH1 complexes

Pelleted ICM were resuspended in 50 mM Tris-HCl pH 8 and homogenised before being solubilised in 2% (w/v) β-DDM. RC-LH1 complexes were purified by a round of anion exchange on a 150 ml diethylaminoethanol (DEAE) Sepharose column at 5 ml min^{-1}, using a gradient of 200–300 mM NaCl in 20 mM Tris-HCl pH 8 with 0.03% (w/v) β-DDM. After spin concentration using 100-kDa molecular weight cut-off (MWCO) concentrators (Thermo Fisher), gel filtration chromatography was carried out on a HiLoad® 16/600 Superdex® 200 pg column (Cytiva) in 50 mM Tris-HCl pH 8 with 200 mM NaCl and 0.03% (w/v) β-DDM at a flow rate of 0.5 ml min^{-1}.

Purification of RC-only complexes

RC-only complexes containing spheroidenone were purified from E9 pBBRBB-*Ppuf*$_{843-1200}$ :: *pufLM* transconjugants grown semi-aerobically as described earlier. Cells were pelleted and lysed as described earlier but, rather than preparing ICM, membranes were harvested from clarified lysate by ultracentrifugation at 185,500×g for 2 h at 4°C in a type 45 Ti ultracentrifuge rotor (Beckman) and transferred to a small Duran bottle containing 100 ml 50 mM Tris-HCl pH 8. These membranes were resuspended and solubilised at room temperature by stirring in the presence of 1% (v/v) LDAO, deliberately harsh conditions to remove other membrane proteins in the mixture. After loading onto a homemade 150 ml DEAE Sepharose column, RCs were purified by anion exchange in 20 mM Tris-HCl pH 8 with 0.1% (v/v) LDAO using a 160–240 mM NaCl gradient, and a 5 ml min^{-1} flow rate on an ÄKTA Prime FPLC (Cytiva). Purified eluate was spin concentrated to <0.5 ml with 50-kDa MWCO centrifugal concentrators (Sartorius) and then purified further by gel filtration at 0.5 ml min^{-1} on a HiLoad® 16/600 Superdex® 200 pg column (Cytiva) into 50 mM Tris-HCl pH 7.5, with 100 mM NaCl and 0.03% (w/v) β-DDM.

RCs containing spheroidene were purified from RC-LH1 complexes (see above) from anaerobic, phototrophically grown strains, by harnessing the sensitivity of LH1 αβ subunit pairs to LDAO treatment. RC-LH1 complexes were buffer-exchanged into 50 mM Tris-HCl buffer at pH 8 with 0.1% (v/v) LDAO and loaded onto a 5ml Q Sepharose column (Cytiva). Bound complexes were then washed with at least 10 column volumes of the same buffer with 4% (v/v) LDAO, before RC-only complexes were eluted using 20 mM Tris-HCl at pH 8 with 0.1% (v/v) LDAO and a 200–400 mM NaCl gradient at a flow rate of 5 ml min^{-1}.

Purification of *c*-type cytochromes from *Rba. sphaeroides*

All three untagged cytochromes (cyt c_2, iso c_2 and cyt c_6) were purified from their respective transconjugant strains by first performing a novel deoxycholate-based fractionation technique, which efficiently separated the contents of the periplasm from the bulk of the cellular proteome. Although the downstream purification steps varied between the four proteins, the periplasmic extraction process was the same each time. The 1.6-L semi-aerobic cultures were pelleted at 4200×g for 30 min at 4°C and resuspended in ~20 ml periplasmic extraction buffer to a total volume of 40 ml, supplemented with EDTA-free protease inhibitor (Merck). This buffer, which was carefully designed to avoid whole cell lysis and deoxycholate hydrogel formation, contained 100 mM HEPES at pH 8 for the two *Rba. sphaeroides* proteins or 100 mM CHES at pH 9 for cyt c_6, along with 500 mM sucrose and 50 mM NaCl as osmotic stabilisers. 0.8 g solid sodium deoxycholate was added to each cell suspension to make a 2% (w/v) solution, which was then incubated in the dark at 4°C with mild agitation. After an hour, spheroplasts were pelleted at 35,000×g for 30 min at 4°C, and the supernatant, which contains the contents of the periplasm, was taken forward to the next step (see below for specific details for each protein). Once purified, each redox carrier protein was concentrated to 2.5 ml in 3-kDa MWCO spin concentrators (Thermo Fisher Scientific), reduced with sodium dithionite and exchanged into the desired buffer using PD-10 desalting columns (Cytiva) according to the manufacturer's instructions.

Purification of untagged cyt c_2

Harnessing the propensity of divalent cations to precipitate bile acids, deoxycholate was removed from the periplasmic fraction by the addition of 6.25 ml 5× deoxycholate precipitation solution (1 M ammonium acetate at pH 5 and 250 mM $MgSO_4$), mixing by inverting the tube and centrifugation at 35,000×g for 30 min at 4°C. The resulting supernatant was then passed through a homemade 30-ml SP Sepharose cation exchange column equilibrated in 50 mM ammonium acetate buffer at pH 5. Any red-coloured eluate was collected, passed through a 0.22-μm filter, diluted 2.5-fold in 50 mM ammonium acetate at pH 5 and clarified by centrifugation at 15,000×g for 10 min at 4°C, whilst the column was washed with successive column volumes of 1 M NaCl, 1 M NaOH and 100% ethanol. The SP Sepharose column was then re-equilibrated in 50 mM ammonium acetate at pH 5, and the clarified coloured eluate loaded onto the column for a second time, resulting in binding of the target protein. Pure cyt c_2 was eluted over a gradient of 60–160 mM NaCl at 5 ml min^{-1} (Supplementary Figure S5).

Purification of untagged iso c_2

With its similar electrostatic properties, untagged iso c_2 was purified using the same column and buffer system used for cyt c_2. Following an identical deoxycholate precipitation step and centrifugation, clarified iso c_2 supernatant was passed through a 0.22-μm filter (Sartorius), diluted ten-fold with 50 mM ammonium acetate buffer at pH 5 and loaded directly onto the column. Cation exchange was performed to elute pure iso c_2 over a 150–250-mM NaCl gradient at 5 ml min^{-1} (Supplementary Figure S5).

Purification of untagged cyt c_6

The much lower surface charge density of the *Synechocystis* redox carrier proteins necessitated a different purification strategy. Instead of adding precipitation buffer, the periplasmic fraction containing cyt c_6 was clarified a second time at 35,000×g for 30 min, then passed through a 0.22-μm filter (Sartorius) and concentrated to ~10 ml in a 3-kDa MWCO spin concentrator (ThermoFisher). The concentrated cytochrome solution was then loaded onto a Hiprep 26/60 Sephacryl S-200 HR column (Cytiva) equilibrated in 50 mM CHES at pH 9 with 200 mM NaCl and run at 1.3 ml min^{-1}, collecting 5 ml fractions. Any red/pink fractions were pooled and diluted ten-fold in 50 mM Tris pH 9, and then loaded onto a 30-ml Q Sepharose column equilibrated in the same buffer. Anion exchange was then performed to purify cyt c_6 further, using a 30–80 mM NaCl gradient and a flow rate of 5 ml min^{-1} (Supplementary Figure S5).

Purification of Pc from *Rba. sphaeroides*

With the lowest affinity for ion exchange columns, Pc was the most challenging and time-consuming redox carrier to purify from *Rba. sphaeroides*. The redox carrier protein could only be purified from 1.6-L cultures of evolved *petE* transconjugant strains, by first lysing the cells by French press as described earlier. Clarified lysate was then concentrated to ~2 ml in a 3-kDa MWCO spin concentrator (Sartorius) and oxidised by addition of a few grains of potassium ferricyanide. The 2 ml of oxidised cell lysate was then loaded onto a HiLoad® 16/600 Superdex® 200 pg gel filtration column (Cytiva) equilibrated in salt-free 50 mM Tris-HCl pH 9. As this column was run at 0.5 ml min^{-1}, a blue Pc band became visible, along with red and yellow bands. All blue fractions were collected, pooled and diluted ten-fold in salt-free 50 mM Tris-HCl buffer pH 9, and then loaded onto a 30-ml Q Sepharose column for anion exchange over a 25–75 mM NaCl gradient, collecting 5 ml fractions in tubes each containing a small amount of ferricyanide. Once Pc-containing fractions were spectrally identified, pooled and concentrated, a second gel filtration chromatography step was necessary to obtain the desired level of purity, using a Superdex® 75 10/300 GL column (Cytiva) with a running buffer containing 50 mM Tris-HCl pH 8 with 1 M NaCl and a flow rate of 0.3 ml min^{-1}. Untagged Pc was required to verify the full activity of a Strep-tagged isoform from *E. coli* which could be produced in higher yields (see below).

Purification of StrepII-tagged Pc from *E. coli*

To produce enough Pc for kinetic studies, we purified recombinant C-terminally StrepII-tagged Pc produced in *E. coli*. One litre of *E. coli* BL21(DE3) cells transformed with pET28a::*petE*-StrepII was grown at 37°C in a baffled flask with 180-rpm agitation. When the OD_{600} reached 0.6, *petE* expression was

induced by adding isopropyl β-D-1-thiogalactopyranoside (IPTG) to 0.5 mM, along with $CuSO_4$ to a final concentration of 600 μM. Induced cells were incubated at 37°C overnight with 180-rpm agitation and harvested the next day at $4000\times g$ for 30 min at 4°C, and then resuspended in 80 ml 20 mM Tris-HCl pH 7.4 with 250 mM DNAse I, and two tablets of EDTA-free protease inhibitor were added. Sodium deoxycholate was then added to a final concentration of 0.1% (w/v), and the cell suspension was mixed by magnetic stirring for 1 h at room temperature before spheroplasts were removed by centrifugation at $8000\times g$ for 15 min at 4°C. The supernatant was retained, and after addition of several grains of potassium ferricyanide, the periplasmic fraction turned blue and was applied to a 4-ml Strep-Tactin XT 4 Flow column (IBA Lifesciences). The column was washed with 20 mM Tris-HCl pH 7.4, and pure Pc was eluted with a column volume of the same buffer with 50 mM biotin (Supplementary Figure S5). No statistically significant difference in turnover rate was found between untagged and Strep-tagged Pc in steady-state turnover assays with RC complexes (Supplementary Figure S6).

Determination of periplasmic protein concentrations, to assess the relative production levels for periplasmic cytochromes and blue copper proteins

Single colonies were grown to the 80-ml (see methods above) stage under semi-aerobic conditions, and the entire culture was pelleted at $4200\times g$ for 30 min at 4°C, removing the supernatant. Each pellet was then resuspended in 500-μl periplasmic extraction buffer (100 mM HEPES pH 8, 500 mM sucrose and 50 mM NaCl) from a 10-ml stock supplemented with 1 EDTA-free protease inhibitor tablet (Merck). The turbidity of each cell suspension was determined by performing a 200-fold dilution and measuring absorbance at 680 nm. Cells were diluted with periplasmic extraction buffer to make a 1-ml suspension for each strain with a consistent OD_{680} value. 200 μl of a 12% (w/v) sodium deoxycholate stock solution in periplasmic extraction buffer was added to each 1-ml suspension and the tubes were incubated in the dark with gentle agitation for 1 h. Spheroplasts were pelleted in 1.5-ml Eppendorf tubes at $16,000\times g$ for 30 min at 4°C, and 800 μl of each supernatant was transferred to a fresh tube. To remove the deoxycholate from solution, 200 μl 5× deoxycholate precipitation solution (1 M ammonium acetate at pH 5 and 250 mM $MgSO_4$) was added to each 800-μl aliquot and mixed thoroughly by inverting the tubes. Most of the precipitated deoxycholate was removed from solution by centrifugation at $16,000\times g$ for 1 h at 4°C, whilst 10mM stocks of sodium dithionite and potassium ferricyanide were prepared in distilled water. After the centrifugation step, solutions were prepared containing each clarified periplasmic fraction and either 1 mM sodium dithionite or potassium ferricyanide in a 700-μl volume and centrifuged again in Eppendorf tubes at $16,000\times g$ for 3 h at 4°C.

The concentration of each redox carrier was determined by spectrophotometry in identical cuvettes using a Cary 60 spectrophotometer (Agilent Technologies) baselined to the extracted periplasm of the negative control strain (Δ*cycA* Δ*cycI* pBBRBB). Periplasmic extracts were prepared from two 80-ml cultures of this double knockout strain to provide a baseline for transconjugant strains making cytochromes or Pc. For cytochromes, the extract was reduced by 1 mM sodium dithionite, whilst the second extract was oxidised with 1 mM potassium ferricyanide to provide a baseline for measuring the absorption spectra of Pc. Extinction coefficients could then be used to determine the relative concentrations of each redox carrier protein in solution. As the oxidised extinction coefficient for Pc is significantly smaller than the reduced extinction coefficients for the cytochromes in this work, small amounts of baseline drift could have a disproportionate impact on concentration estimates for Pc strains. To account for this, rather than using the raw value, the OD_{597} for each Pc periplasmic extraction was calculated using the formula $(OD_{603}-OD_{700})\times 1.35$, where 1.35 is equal to OD_{597}/OD_{700} of pure Pc. Assuming that the proportion of total molecules localised in the periplasm remains the same for each redox carrier protein with equal uptake into chromatophores, this technique provides a cheap and high-throughput tool for assessing the relative production levels for periplasmic cytochromes and blue copper proteins.

Pyridine hemochromagen assays

To determine the concentration of iso c_2, for which no published extinction coefficients were available, pyridine hemochromagen assays were carried out using the protocol of Barr and Guo [81], using a reduced extinction coefficient of 30.27 $mM^{-1}cm^{-1}$ for the pyr_2-haem *c* co-ordination complex [82]. Absorbance spectra were collected on a Cary 60 spectrophotometer with a 1-cm pathlength, and extinction coefficients

Table 3: Extinction coefficients used in the present study

Species	Wavelength	Extinction coefficient, ε (mM^{-1})	Source
RC-LH1	875	3000	[83]
RC	802	288	[84]
Cyt c_2	550	30.8 (reduced)	[20]
		21.5 (reduced−oxidised)	
Iso c_2	551	25.6 (reduced)	The present study
		19.1 (reduced−oxidised)	
Cyt c_6	552	24.1 (reduced)	[43]
		19.5 (reduced−oxidised)	[85]
Pc	597	4.5 (reduced)	[86]
		4.5 (reduced−oxidised)	
Cyt c	550	27.6 (reduced)	[87]
		21.1 (reduced−oxidised)	
DUQ	278	14 (oxidised in EtOH)	[88]
UQ-2	275	13.7 (oxidised in EtOH)	[88]

Cyt c, cytochrome c. Cyt c_2, cytochrome c_2. Cyt c_6, cytochrome c_6. DUQ, decylubiquinone. Iso c_2, isocytochrome c_2. Pc, plastocyanin. RC, reaction centre. RC-LH1, reaction centre-light harvesting 1. UQ-2, ubiquinone-2.

were calculated for 551 nm, the closest whole number to the reduced peak of the heme c cofactor in iso c_2. This method gave values as follows: $\varepsilon_{551 \, (red)}$=25.6 mM^{-1} cm^{-1}, $\varepsilon_{551 \, (ox)}$=6.53 mM^{-1} cm^{-1} and therefore $\varepsilon_{551 \, (red - ox)}$=19.1 mM^{-1} cm^{-1}.

RC-only and RC-LH1 turnover assays

Turnover assays were conducted under steady-state conditions in a similar fashion to those described in Martin et al. [53], using 3×300 μl solutions containing RC or RC-LH1, soluble redox carrier protein and quinone, in a solution containing 0.03% (w/v) β-DDM and, where necessary, 1 mM sodium D-ascorbate to keep cytochromes reduced. Each pre-reduced soluble redox carrier protein was added to a concentration at least 20-fold higher than the RC/RC-LH1 complex in solution. Quinones were added in excess from ethanol stock solutions to a final assay concentration of 50 μM, using a volume of <2 μl to minimise the amount of ethanol in solution.

Following overnight dark adaptation, each 300 μl reaction mixture was placed in a 3-ml, 1cm pathlength quartz cuvette and monitored at a fixed wavelength using a Cary 60 spectrophotometer (Agilent Technologies). The temperature of the solution was maintained at 25°C by a Cary Single Cell Peltier Accessory (Agilent Technologies). Ten seconds into data recording, excitation energy was delivered via a fibre optic cable from an 810-nm M810F2 LED (Thorlabs Ltd., U.K), typically driven at 100% intensity using a DC2200 controller (Thorlabs Ltd., U.K) for 20–50 s. Depending on how rapidly the signal changed, the data were processed by fitting the linear initial rate over 0.025–5 s, starting from the first data point where the absorbance started dropping continuously. Rates were normalised to e$^-$/RC/s by dividing the initial rate by the reduced minus oxidised extinction coefficient for the redox carrier protein (Table 3), and then by the RC or RC-LH1 concentration. All cytochrome extinction coefficients are from either *Rba. sphaeroides* or *Synechocystis* sp. PCC 6803, whilst in the absence of a published extinction coefficient for Pc from *Synechocystis* sp. PCC 6803, the ε_{597} from *Phaseolus vulgaris* (common bean) was used instead [86].

Data Availability

Any data not provided within the paper as a table, figure or supplementary file is available from the corresponding authors upon request.

Competing Interests

The authors declare that there are no competing interests associated with the manuscript.

Funding

CRediT Author Contribution

Adam G.M. Bowie: Conceptualization, Formal analysis, Investigation, Visualization, Methodology, Writing — original draft, Writing — review and editing. Andrew Hitchcock: Conceptualization, Formal analysis, Investigation, Supervision, Writing — review and editing. Matthew S. Proctor: Investigation. Elizabeth C. Martin: Investigation. David J.K. Swainsbury: Formal Analysis, Supervision, Investigation, Writing — review and editing. C. Neil Hunter: Conceptualization, Formal analysis, Resources, Supervision, Funding acquisition, Writing — review and editing.

Abbreviations

ALE, adaptive laboratory evolution; BChl, bacteriochlorophyll; Chl, chlorophyll; DUQ, decylubiquinone; ICM, intracytoplasmic membranes; LDAO, lauryldimethylamine oxide; LED, light-emitting diode; MWCO, molecular weight cut-off; PQ, plastoquinone; PSI, photosystem I; PSII, photosystem II; PSIII, photosystem III; Pc, plastocyanin; RC, reaction centre; RC-LH1, reaction centre-light harvesting 1; *Rba.*, *Rhodobacter*; UQ, Ubiquinone; WT, wildtype; cryo-EM, cryogenic electron microscopy; cyt bc_1, cytochrome bc_1; cyt b_6f, cytochrome b_6f; cyt c, cytochrome c; cyt c_2, cytochrome c_2; cyt c_6, cytochrome c_6; iso c_2, isocytochrome c_2; vdW, van der Waals.

References

1   Blankenship, R.E. (1992) Origin and early evolution of photosynthesis. *Photosyn. Res.* **33**, 91–111 https://doi.org/10.1007/BF00039173 PMID: 11538390

2   Sadekar, S., Raymond, J. and Blankenship, R.E. (2006) Conservation of distantly related membrane proteins: photosynthetic reaction centers share a common structural core. *Mol. Biol. Evol.* **23**, 2001–2007 https://doi.org/10.1093/molbev/msl079 PMID: 16887904

3   Orf, G.S., Gisriel, C. and Redding, K.E. (2018) Evolution of photosynthetic reaction centers: insights from the structure of the heliobacterial reaction center. *Photosyn. Res.* **138**, 11–37 https://doi.org/10.1007/s11120-018-0503-2 PMID: 29603081

4   Cardona, T., Sánchez-Baracaldo, P., Rutherford, A.W. and Larkum, A.W. (2019) Early archean origin of photosystem II. *Geobiology* **17**, 127–150 https://doi.org/10.1111/gbi.12322 PMID: 30411862

5   Raymond, J. and Blankenship, R.E. (2008) The origin of the oxygen-evolving complex. *Coord. Chem. Rev.* **252**, 377–383 https://doi.org/10.1016/j.ccr.2007.08.026

6   Canfield, D.E., Ngombi-Pemba, L., Hammarlund, E.U., Bengtson, S., Chaussidon, M., Gauthier-Lafaye, F, et al. (2013) Oxygen dynamics in the aftermath of the Great Oxidation of Earth's atmosphere. *Proc. Natl. Acad. Sci. U.S.A* **110**, 16736–16741 https://doi.org/10.1073/pnas.1315570110

7   Blankenship, R.E. (2014) *Molecular Mechanisms of Photosynthesis*, 2nd ed ed, Hoboken, John Wiley & Sons Incorporated

8   Johnson, M.P. (2016) Photosynthesis. *Essays Biochem.* **60**, 255–273 https://doi.org/10.1042/EBC20160016 PMID: 27784776

9   Blankenship, R.E., Tiede, D.M., Barber, J., Brudvig, G.W., Fleming, G., Ghirardi, M. et al. (2011) Comparing photosynthetic and photovoltaic efficiencies and recognizing the potential for improvement. *Science* **332**, 805–809 https://doi.org/10.1126/science.1200165

10   Ort, D.R., Merchant, S.S., Alric, J., Barkan, A., Blankenship, R.E., Bock, R. et al. (2015) Redesigning photosynthesis to sustainably meet global food and bioenergy demand. *Proc. Natl. Acad. Sci. U.S.A.* **112**, 8529–8536 https://doi.org/10.1073/pnas.1424031112 PMID: 26124102

11   Hitchcock, A., Hunter, C.N., Sobotka, R., Komenda, J., Dann, M. and Leister, D. (2022) Redesigning the photosynthetic light reactions to enhance photosynthesis - the PhotoRedesign consortium. *Plant J.* **109**, 23–34 https://doi.org/10.1111/tpj.15552 PMID: 34709696

12   Leister, D. (2023) Enhancing the light reactions of photosynthesis: strategies, controversies, and perspectives. *Mol. Plant* **16**, 4–22 https://doi.org/10.1016/j.molp.2022.08.005

13   Zhao, Z., Vercellino, I., Knoppová, J., Sobotka, R., Murray, J.W., Nixon, P.J. et al. (2023) The Ycf48 accessory factor occupies the site of the oxygen-evolving manganese cluster during photosystem II biogenesis. *Nat. Commun.* **14**, 4681 https://doi.org/10.1038/s41467-023-40388-6

14   Gisriel, C.J., Wang, J., Liu, J., Flesher, D.A., Reiss, K.M., Huang, H.-L. et al. (2022) High-resolution cryo-electron microscopy structure of photosystem II from the mesophilic cyanobacterium, *Synechocystis* sp. PCC 6803. *Proc. Natl. Acad. Sci. U.S.A* **119**, e2116765118 https://doi.org/10.1073/pnas.2116765118

15   Proctor, M.S., Malone, L.A., Farmer, D.A., Swainsbury, D.J.K., Hawkings, F.R., Pastorelli, F. et al. (2022) Cryo-EM structures of the Synechocystis sp. PCC 6803 cytochrome b_6f complex with and without the regulatory PetP subunit. *Biochem. J.* **479**, 1487–1503 https://doi.org/10.1042/BCJ20220124 PMID: 35726684

PORTLAND
PRESS

16 Qian, P., Swainsbury, D.J.K., Croll, T.I., Salisbury, J.H., Martin, E.C., Jackson, P.J. et al. (2021) Cryo-EM structure of the monomeric *Rhodobacter sphaeroides* RC-LH1 core complex at 2.5 Å. *Biochem. J.* **478**, 3775–3790 https://doi.org/10.1042/BCJ20210631 PMID: 34590677

17 Hitchcock, A., Hunter, C.N. and Canniffe, D.P. (2020) Progress and challenges in engineering cyanobacteria as chassis for light-driven biotechnology. *Microb. Biotechnol.* **13**, 363–367 https://doi.org/10.1111/1751-7915.13526 PMID: 31880868

18 Schierenbeck, L., Ries, D., Rogge, K., Grewe, S., Weisshaar, B. and Kruse, O. (2015) Fast forward genetics to identify mutations causing a high light tolerant phenotype in *Chlamydomonas reinhardtii* by whole-genome-sequencing. *BMC Genomics* **16**, 57 https://doi.org/10.1186/s12864-015-1232-y PMID: 25730202

19 Dann, M., Ortiz, E.M., Thomas, M., Guljamow, A., Lehmann, M., Schaefer, H. et al. (2021) Enhancing photosynthesis at high light levels by adaptive laboratory evolution. *Nat. Plants* **7**, 681–695 https://doi.org/10.1038/s41477-021-00904-2

20 Axelrod, H.L., Abresch, E.C., Okamura, M.Y., Yeh, A.P., Rees, D.C. and Feher, G. (2002) X-ray structure determination of the cytochrome c_2: reaction center electron transfer complex from *Rhodobacter sphaeroides*. *J. Mol. Biol.* **319**, 501–515 https://doi.org/10.1016/S0022-2836(02)00168-7 PMID: 12051924

21 Busch, A. and Hippler, M. (2011) The structure and function of eukaryotic photosystem I. *Biochimica et Biophysica Acta (BBA) - Bioenergetics* **1807**, 864–877 https://doi.org/10.1016/j.bbabio.2010.09.009

22 Wachtveitl, J., Farchaus, J.W., Mathis, P. and Oesterhelt, D. (1993) Tyrosine 162 of the photosynthetic reaction center L-subunit plays a critical role in the cytochrome c_2 mediated rereduction of the photooxidized bacteriochlorophyll dimer in *Rhodobacter sphaeroides*. 2. Quantitative kinetic analysis. *Biochemistry* **32**, 10894–10904 https://doi.org/10.1021/bi00091a045 PMID: 8399239

23 Farchaus, J.W., Wachtveitl, J., Mathis, P. and Oesterhelt, D. (1993) Tyrosine 162 of the photosynthetic reaction center L-subunit plays a critical role in the cytochrome c_2 mediated rereduction of the photooxidized bacteriochlorophyll dimer in *Rhodobacter sphaeroides*. 1. Site-directed mutagenesis and initial characterization. *Biochemistry* **32**, 10885–10893 https://doi.org/10.1021/bi00091a044 PMID: 8399238

24 Jordan, P., Fromme, P., Witt, H.T., Klukas, O., Saenger, W. and Krauß, N. (2001) Three-dimensional structure of cyanobacterial photosystem I at 2.5 Å resolution. *Nature* **411**, 909–917 https://doi.org/10.1038/35082000

25 Sommer, F., Drepper, F. and Hippler, M. (2002) The luminal helix l of PsaB is essential for recognition of plastocyanin or cytochrome c_6 and fast electron transfer to photosystem I in *Chlamydomonas reinhardtii*. *J. Biol. Chem.* **277**, 6573–6581 https://doi.org/10.1074/jbc.M110633200

26 Sommer, F., Drepper, F., Haehnel, W. and Hippler, M. (2004) The Hydrophobic recognition Site formed by residues PsaA-Trp651 and PsaB-Trp627 of Photosystem I in *Chlamydomonas reinhardtii* confers distinct selectivity for binding of plastocyanin and cytochrome c_6. *J. Biol. Chem.* **279**, 20009–20017 https://doi.org/10.1074/jbc.M313986200

27 Axelrod, H.L. and Okamura, M.Y. (2005) The structure and function of the cytochrome c_2: reaction center electron transfer complex from *Rhodobacter sphaeroides*. *Photosyn. Res.* **85**, 101–114 https://doi.org/10.1007/s11120-005-1368-8 PMID: 15977062

28 Vasilev, C., Nguyen, J., Bowie, A.G.M., Mayneord, G.E., Martin, E.C., Hitchcock, A. et al. (2024) Single-molecule detection of the encounter and productive electron transfer complexes of a photosynthetic reaction center. *J. Am. Chem. Soc.* **146**, 20019–20032 https://doi.org/10.1021/jacs.4c03913

29 Caspy, I., Fadeeva, M., Kuhlgert, S., Borovikova-Sheinker, A., Klaiman, D., Masrati, G. et al. (2021) Structure of plant photosystem I-plastocyanin complex reveals strong hydrophobic interactions. *Biochem. J.* **478**, 2371–2384 https://doi.org/10.1042/BCJ20210267 PMID: 34085703

30 Redinbo, M.R., Yeates, T.O. and Merchant, S. (1994) Plastocyanin: structural and functional analysis. *J. Bioenerg. Biomembr.* **26**, 49–66 https://doi.org/10.1007/BF00763219 PMID: 8027022

31 Ramesh, V.M., Guergova-Kuras, M., Joliot, P. and Webber, A.N. (2002) Electron transfer from plastocyanin to the photosystem I reaction center in mutants with increased potential of the primary donor in *Chlamydomonas reinhardtii*. *Biochemistry* **41**, 14652–14658 https://doi.org/10.1021/bi026392z

32 Díaz-Quintana, A., Navarro, J.A., Hervás, M., Molina-Heredia, F.P., De la Cerda, B. and De la Rosa, M.A. (2003) A comparative structural and functional analysis of cyanobacterial plastocyanin and cytochrome c_6 as alternative electron donors to Photosystem I. *Photosyn. Res.* **75**, 97–110 https://doi.org/10.1023/A:1022841513592

33 Frazão, C., Soares, C.M., Carrondo, M.A., Pohl, E., Dauter, Z., Wilson, K.S. et al. (1995) Ab initio determination of the crystal structure of cytochrome c_6 and comparison with plastocyanin. *Structure* **3**, 1159–1169 https://doi.org/10.1016/S0969-2126(01)00252-0

34 De la Cerda, B., Castielli, O., Duran, R.V., Navarro, J.A., Hervas, M. and De la Rosa, M.A. (2007) A proteomic approach to iron and copper homeostasis in cyanobacteria. *Brief. Funct. Genomic. Proteomic.* **6**, 322–329 https://doi.org/10.1093/bfgp/elm030

35 Aitken, A. (1975) Prokaryote-eukaryote relationship and the amino acid sequence of plastocyanin from *Anabaena variabilis*. *Biochem. J.* **149**, 675–683 https://doi.org/10.1042/bj1490675 PMID: 812489

36 Chitnis, P.R., Purvis, D. and Nelson, N. (1991) Molecular cloning and targeted mutagenesis of the gene *psaF* encoding subunit III of photosystem I from the cyanobacterium *Synechocystis* sp. PCC 6803. *J. Biol. Chem* **266**, 20146–20151 https://doi.org/10.1016/S0021-9258(18)54902-4 PMID: 1939076

37 Hope, A.B. (2000) Electron transfers amongst cytochrome f, plastocyanin and photosystem I: kinetics and mechanisms. *Biochimica et Biophysica Acta (BBA) - Bioenergetics* **1456**, 5–26 https://doi.org/10.1016/S0005-2728(99)00101-2

38 Moser, C.C., Keske, J.M., Warncke, K., Farid, R.S. and Dutton, P.L. (1992) Nature of biological electron transfer. *Nature* **355**, 796–802 https://doi.org/10.1038/355796a0

39 Page, C.C., Moser, C.C., Chen, X. and Dutton, P.L. (1999) Natural engineering principles of electron tunnelling in biological oxidation–reduction. *Nature* **402**, 47–52 https://doi.org/10.1038/46972

40 Moser, C.C., Anderson, J.L.R. and Dutton, P.L. (2010) Guidelines for tunneling in enzymes. *Biochimica et Biophysica Acta (BBA) - Bioenergetics* **1797**, 1573–1586 https://doi.org/10.1016/j.bbabio.2010.04.441

41 Abramson, J., Adler, J., Dunger, J., Evans, R., Green, T., Pritzel, A. et al. (2024) Accurate structure prediction of biomolecular interactions with AlphaFold 3. *Nature* **630**, 493–500 https://doi.org/10.1038/s41586-024-07487-w

42 Rott, M.A. and Donohue, T.J. (1990) *Rhodobacter sphaeroides* spd mutations allow cytochrome c_2-independent photosynthetic growth. *J. Bacteriol.* **172**, 1954–1961 https://doi.org/10.1128/jb.172.4.1954-1961.1990

43 Díaz, A., Navarro, F., Hervás, M., Navarro, J.A., Chávez, S., Florencio, F.J. et al. (1994) Cloning and correct expression in *E. coli* of the *petJ* gene encoding cytochrome c_6 from *Synechocystis* 6803. *FEBS Lett.* **347**, 173–177 https://doi.org/10.1016/0014-5793(94)00529-x PMID: 8033998

44 Pettigrew, G.W., Meyer, T.E., Bartsch, R.G. and Kamen, M.D. (1976) pH dependence of the oxidation-reduction potential of cytochrome c_2. *Biochimica et Biophysica Acta (BBA) - Bioenergetics* **430**, 197–208 https://doi.org/10.1016/0005-2728(76)90079-7

45 Rott, M.A., Fitch, J., Meyer, T.E. and Donohue, T.J. (1992) Regulation of a cytochrome c_2 isoform in wild-type and cytochrome c_2 mutant strains of *Rhodobacter sphaeroides*. *Arch. Biochem. Biophys.* **292**, 576–582 https://doi.org/10.1016/0003-9861(92)90033-s PMID: 1309978

46 Honorato, R.V., Koukos, P.I., Jiménez-García, B., Tsaregorodtsev, A., Verlato, M., Giachetti, A. et al. (2021) Structural biology in the clouds: the WeNMR-EOSC ecosystem. *Front. Mol. Biosci.* **8**, 729513 https://doi.org/10.3389/fmolb.2021.729513 PMID: 34395534

47 Honorato, R.V., Roel-Touris, J. and Bonvin, A.M.J.J. (2019) MARTINI-based protein-DNA coarse-grained HADDOCKing. *Front. Mol. Biosci.* **6**, 102 https://doi.org/10.3389/fmolb.2019.00102 PMID: 31632986

48 Jumper, J., Evans, R., Pritzel, A., Green, T., Figurnov, M., Ronneberger, O. et al. (2021) Highly accurate protein structure prediction with AlphaFold. *Nature New Biol.* **596**, 583–589 https://doi.org/10.1038/s41586-021-03819-2

49 Jurrus, E., Engel, D., Star, K., Monson, K., Brandi, J., Felberg, L.E. et al. (2018) Improvements to the APBS biomolecular solvation software suite. *Protein Sci.* **27**, 112–128 https://doi.org/10.1002/pro.3280 PMID: 28836357

50 Visschers, R.W., Vulto, S.I.E., Jones, M.R., Grondelle, R. van and Kraayenhof, R. (1999) Functional LH1 antenna complexes influence electron transfer in bacterial photosynthetic reaction centers. *Photosyn. Res.* **59**, 95–104 https://doi.org/10.1023/A:1006169201579

51 Nakamura, A., Suzawa, T., Kato, Y. and Watanabe, T. (2011) Species dependence of the redox potential of the primary electron donor P700 in photosystem I of oxygenic photosynthetic organisms revealed by spectroelectrochemistry. *Plant Cell Physiol.* **52**, 815–823 https://doi.org/10.1093/pcp/pcr034 PMID: 21429906

52 Lin, X., Williams, J.C., Allen, J.P. and Mathis, P. (1994) Relationship between rate and free energy difference for electron transfer from cytochrome c_2 to the reaction center in Rhodobacter sphaeroides. *Biochemistry* **33**, 13517–13523 https://doi.org/10.1021/bi00250a002

53 Martin, E.C., Bowie, A.G.M., Wellfare Reid, T., Hunter, C. N., Hitchcock, A. and Swainsbury, D.J.K. (2024) Sulfoquinovosyl diacylglycerol is required for dimerisation of the *Rhodobacter sphaeroides* reaction centre-light harvesting 1 core complex. *Biochem. J.* **481**, 823–838 https://doi.org/10.1042/BCJ20240125 PMID: 38780411

54 Tikh, I.B., Held, M. and Schmidt-Dannert, C. (2014) BioBrick™ compatible vector system for protein expression in *Rhodobacter sphaeroides*. *Appl. Microbiol. Biotechnol.* **98**, 3111–3119 https://doi.org/10.1007/s00253-014-5527-8 PMID: 24509770

55 Witthuhn, V.C., Gao, J., Hong, S., Halls, S., Rott, M.A., Wraight, C.A, et al. (1997) Reactions of isocytochrome c_2 in the photosynthetic electron transfer chain of *Rhodobacter sphaeroides*. *Biochemistry* **36**, 903–911 https://doi.org/10.1021/bi961648k

56 Lilburn, T.G., Haith, C.E., Prince, R.C. and Beatty, J.T. (1992) Pleiotropic effects of *pufX* gene deletion on the structure and function of the photosynthetic apparatus of *Rhodobacter capsulatus*. *Biochimica et Biophysica Acta (BBA) - Bioenergetics* **1100**, 160–170 https://doi.org/10.1016/0005-2728(92)90077-f PMID: 1319207

57 Chidgey, J.W., Jackson, P.J., Dickman, M.J. and Hunter, C.N. (2017) PufQ regulates porphyrin flux at the haem/bacteriochlorophyll branchpoint of tetrapyrrole biosynthesis via interactions with ferrochelatase. *Mol. Microbiol.* **106**, 961–975 https://doi.org/10.1111/mmi.13861 PMID: 29030914

58 Overfield, R.E., Wraight, C.A. and Devault, D. (1979) Microsecond photooxidation kinetics of cytochrome c_2 from *Rhodopseudomonas sphaeroides*: *in vivo* and solution studies. *FEBS Lett.* **105**, 137–142 https://doi.org/10.1016/0014-5793(79)80903-5 PMID: 226405

59 Gerencsér, L., Laczkó, G. and Maróti, P. (1999) Unbinding of Oxidized Cytochrome *c* from Photosynthetic Reaction Center of *Rhodobacter sphaeroides* Is the bottleneck of fast turnover. *Biochemistry* **38**, 16866–16875 https://doi.org/10.1021/bi991563u

60 Reed, D.W. and Clayton, R.K. (1968) Isolation of a reaction center fraction from *Rhodopseudomonas spheroides*. *Biochem. Biophys. Res. Commun.* **30**, 471–475 https://doi.org/10.1016/0006-291x(68)90075-2 PMID: 5645432

61 Peschek, G.A. (1999) *Photosynthesis and Respiration of Cyanobacteria*. In *In the Phototrophic Prokaryotes* (W. Löffelhardt and G. Schmetterer, eds), Springer US, https://doi.org/10.1007/978-1-4615-4827-0_24

62 Hervás, M., Navarro, J.A. and De la Rosa, M.A. (2003) Electron Transfer between Membrane Complexes and Soluble Proteins in Photosynthesis. *Acc. Chem. Res.* **36**, 798–805 https://doi.org/10.1021/ar020084b

63 Drepper, F., Hippler, M., Nitschke, W. and Haehnel, W. (1996) Binding dynamics and electron transfer between plastocyanin and photosystem I. *Biochemistry* **35**, 1282–1295 https://doi.org/10.1021/bi951471e

64 Tetreault, M., Rongey, S.H., Feher, G. and Okamura, M.Y. (2001) Interaction between cytochrome c_2 and the photosynthetic reaction center from *Rhodobacter sphaeroides*: effects of charge-modifying mutations on binding and electron transfer. *Biochemistry* **40**, 8452–8462 https://doi.org/10.1021/bi010222p

65 Swainsbury, D.J.K., Qian, P., Jackson, P.J., Faries, K.M., Niedzwiedzki, D.M., Martin, E.C. et al. (2021) Structures of *Rhodopseudomonas palustris* RC-LH1 complexes with open or closed quinone channels. *Sci. Adv.* **7**, eabe2631 https://doi.org/10.1126/sciadv.abe2631

66 Mao, R., Guo, J., Bie, L., Liu, L.-N. and Gao, J. (2024) Tunneling mechanisms of quinones in photosynthetic reaction center-light harvesting 1 supercomplexes. *Small Sci.* **4**, 2400188 https://doi.org/10.1002/smsc.202400188 PMID: 40213462

67 Swainsbury, D.J.K., Qian, P., Hitchcock, A. and Hunter, C.N. (2023) The structure and assembly of reaction centre-light-harvesting 1 complexes in photosynthetic bacteria. *Biosci. Rep.* **43**, BSR20220089 https://doi.org/10.1042/BSR20220089 PMID: 37098760

68 Qian, P., Papiz, M.Z., Jackson, P.J., Brindley, A.A., Ng, I.W., Olsen, J.D. et al. (2013) Three-dimensional structure of the *Rhodobacter sphaeroides* RC-LH1-PufX Complex: dimerization and quinone channels promoted by PufX. *Biochemistry* **52**, 7575–7585 https://doi.org/10.1021/bi4011946

69 Semchonok, D.A., Siponen, M.I., Tüting, C., Charras, Q., Kyrilis, F.L., Hamdi, F, et al. (2022) Cryo-EM structure of the *Rhodobaca bogoriensis* RC-LH1-PufX dimeric complex at 2.9 Å [bioRxiv]. https://doi.org/10.1101/2022.02.25.481955

70 Tani, K., Kanno, R., Kikuchi, R., Kawamura, S., Nagashima, K.V.P., Hall, M. et al. (2022) Asymmetric structure of the native *Rhodobacter sphaeroides* dimeric LH1–RC complex. *Nat. Commun.* **13** https://doi.org/10.1038/s41467-022-29453-8

71 Cao, P., Bracun, L., Yamagata, A., Christianson, B.M., Negami, T., Zou, B. et al. (2022) Structural basis for the assembly and quinone transport mechanisms of the dimeric photosynthetic RC-LH1 supercomplex. *Nat. Commun.* **13**, 1977 https://doi.org/10.1038/s41467-022-29563-3 PMID: 35418573

72   Geyer, T. and Helms, V. (2006) Reconstruction of a kinetic model of the chromatophore vesicles from *Rhodobacter sphaeroides*. *Biophys. J.* **91**, 927–937 https://doi.org/10.1529/biophysj.105.067561 PMID: 16714340

73   Cartron, M.L., Olsen, J.D., Sener, M., Jackson, P.J., Brindley, A.A., Qian, P. et al. (2014) Integration of energy and electron transfer processes in the photosynthetic membrane of *Rhodobacter sphaeroides*. *Biochimica et Biophysica Acta (BBA) - Bioenergetics* **1837**, 1769–1780 https://doi.org/10.1016/j.bbabio.2014.02.003

74   Sener, M., Strumpfer, J., Singharoy, A., Hunter, C.N. and Schulten, K. (2016) Overall energy conversion efficiency of a photosynthetic vesicle. *Elife* **5**, e09541 https://doi.org/10.7554/eLife.09541

75   Vasilev, C., Mayneord, G.E., Brindley, A.A., Johnson, M.P. and Hunter, C.N. (2019) Dissecting the cytochrome c_2-reaction centre interaction in bacterial photosynthesis using single molecule force spectroscopy. *Biochem. J.* **476**, 2173–2190 https://doi.org/10.1042/BCJ20170519 PMID: 31320503

76   Swainsbury, D.J.K., Martin, E.C., Vasilev, C., Parkes-Loach, P.S., Loach, P.A. and Hunter, C. N.. (2017) Engineering of a calcium-ion binding site into the RC-LH1-PufX complex of *Rhodobacter sphaeroides* to enable ion-dependent spectral red-shifting. *Biochimica et Biophysica Acta (BBA) - Bioenergetics* **1858**, 927–938 https://doi.org/10.1016/j.bbabio.2017.08.009

77   Qian, P., Martin, E.C., Ng, I.W. and Hunter, C.N. (2017) The C-terminus of PufX plays a key role in dimerisation and assembly of the reaction center light-harvesting 1 complex from *Rhodobacter sphaeroides*. *Biochimica et Biophysica Acta (BBA) - Bioenergetics* **1858**, 795–803 https://doi.org/10.1016/j.bbabio.2017.06.001

78   Simon, R., Priefer, U. and Pühler, A. (1983) A broad host range mobilization system for *in vivo* genetic engineering: transposon mutagenesis in gram negative bacteria. *Biotechnology (N.Y.)* **1**, 784–791 https://doi.org/10.1038/nbt1183-784

79   Sutherland, G.A., Qian, P., Hunter, C.N., Swainsbury, D.J.K. and Hitchcock, A. (2022) Chapter five - engineering purple bacterial carotenoid biosynthesis to study the roles of carotenoids in light-harvesting complexes. In *Methods in Enzymology* (E.T. Wurtzel, ed), pp. 137–184, Academic Press, https://doi.org/10.1016/bs.mie.2022.04.001

80   Hunter, C.N. and Turner, G. (1988) Transfer of genes coding for apoproteins of reaction centre and light-harvesting LH1 complexes to *Rhodobacter sphaeroides*. *Microbiology (Reading, Engl.)* **134**, 1471–1480 https://doi.org/10.1099/00221287-134-6-1471

81   Barr, I. and Guo, F. (2015) Pyridine hemochromagen assay for determining the concentration of heme in purified protein solutions. *Bio Protoc.* **5**, e1594 https://doi.org/10.21769/bioprotoc.1594 PMID: 27390766

82   Berry, E.A. and Trumpower, B.L. (1987) Simultaneous determination of hemes *a*, *b*, and *c* from pyridine hemochrome spectra. *Anal. Biochem.* **161**, 1–15 https://doi.org/10.1016/0003-2697(87)90643-9 PMID: 3578775

83   Huang, X., Vasilev, C., Swainsbury, D.J.K. and Hunter, C.N. (2024) Excitation energy transfer in proteoliposomes reconstituted with LH2 and RC-LH1 complexes from *Rhodobacter sphaeroides*. *Biosci. Rep.* **44**, BSR20231302 https://doi.org/10.1042/BSR20231302 PMID: 38227291

84   Straley, S.C., Parson, W.W., Mauzerall, D.C. and Clayton, R.K. (1973) Pigment content and molar extinction coefficients of photochemical reaction centers from *Rhodopseudomonas spheroides*. *Biochimica et Biophysica Acta (BBA) - Bioenergetics* **305**, 597–609 https://doi.org/10.1016/0005-2728(73)90079-0

85   Cho, Y.S., Wang, Q.J., Krogmann, D. and Whitmarsh, J. (1999) Extinction coefficients and midpoint potentials of cytochrome c_6 from the cyanobacteria *Arthrospira maxima*, *Microcystis aeruginosa*, and *Synechocystis* 6803. *Biochimica et Biophysica Acta (BBA) - Bioenergetics* **1413**, 92–97 https://doi.org/10.1016/S0005-2736(99)00124-8

86   Milne, P.R. and Wells, J.R.E. (1970) Structural and molecular weight studies on the small copper protein, plastocyanin. *J. Biol. Chem.* **245**, 1566–1574 https://doi.org/10.1016/S0021-9258(19)77132-4

87   Margoliash, E. and Walasek, O.F. (1967) Cytochrome *c* from vertebrate and invertebrate sources. In *Methods in Enzymology*, pp. 339–348, Academic Press, https://doi.org/10.1016/0076-6879(67)10064-5

88   Fato, R., Estornell, E., Di Bernardo, S., Pallotti, F., Parenti Castelli, G. and Lenaz, G. (1996) Steady-state kinetics of the reduction of coenzyme Q analogs by complex I (NADH:ubiquinone oxidoreductase) in bovine heart mitochondria and submitochondrial particles. *Biochemistry* **35**, 2705–2716 https://doi.org/10.1021/bi9516034